# Controlled Coronal Stiffness Prosthetic Ankle for Improving Balance on Uneven Terrain

Jeffrey J. Gorges

A thesis submitted in

partial fulfillment of the requirements

for the degree of

Master of Science in Mechanical Engineering

University of Washington

2013

Committee:

Glenn Klute, PhD

Randal Ching, PhD

Santosh Devasia, PhD

Program Authorized to Offer Degree:

Mechanical Engineering

University of Washington

## Abstract

Controlled Coronal Stiffness Prosthetic Ankle for Improved Balance on Uneven Terrain

Jeffrey Gorges

Chair of the Supervisory Committee:

Glenn Klute, Ph.D.

Affiliate Associate Professor, Departments of Mechanical and Electrical Engineering

### *Background*

For lower limb amputees, quality of life is directly related to the functionality of their prosthetic devices. Uneven terrain can cause significant disturbances to an individual's gait. Disturbances with significant inversion or eversion are more likely to cause imbalance than sagittal plane disturbances, yet currently marketed devices do not have controlled methods for reacting in the coronal plane.

The objective of this project was to develop a prosthetic ankle that is capable of changing stiffness characteristics in the coronal plane with the objective of creating a more stable support for amputees. This device will be used in further research to characterize kinematics in the coronal plane and develop strategies of improving amputee balance while traversing uneven terrain.

## *Methods*

A prosthetic ankle was designed, built and tested that is capable of controlling the rotational stiffness of the ankle for inversion and eversion. The effective length of two cantilever beam springs can be changed by a motor controlled through a battery powered on-board computer. A series of bench tests and human subject tests were performed to test the functionality of the device including stiffness characterization, comparison to available commercial devices, motor control characteristics, human subject standing balance center of pressure tracking, and walking on an inverted and everted plane.

## *Results*

Characterization of the device and stiffness properties showed that over a series of springs it was capable of developing a range of rotational stiffness values from 23 Nm/rad to 510 Nm/rad. When placed in series with a stiff commercial foot, one particular set of springs proved to have a greater range of stiffness than that covered by a series of commercial feet. Human subject testing demonstrated methods and metrics that could be used to evaluate optimal stiffness values and profiles. Motor tests showed that the drive system did not perform well enough to quickly change stiffness values while fully weighted on an inverted or everted surface.

## *Conclusions*

The range of stiffness characteristics over which the device is capable has proven to be sufficient. However, the drive system for dynamically changing the stiffness throughout the gait cycle requires a few design changes. The device has proven to be capable of testing the effects of amputee balance and kinematics while walking on uneven terrain. Further use of this device for research will help to develop the optimal coronal stiffness characteristics and controls for improved prosthetic ankles.

# TABLE OF CONTENTS

# List of Figures

# List of Tables

# 1 Background

Lower limb amputees are at a serious disadvantage when navigating uneven terrain. One reason is not being able to control their prosthetic ankle while walking. The current state of the art in lower limb prosthetic devices tends to focus on improving motion, control and energy return in the sagittal plane. Since this is the primary plane of motion in the ankle, this direction of research and advancement makes sense. However, more work needs to be done to improve control and functionality of lower limb prostheses in the coronal plane. In an attempt to replicate the complexity of a biological ankle, improvements must be made. In order to develop marketable devices, more must be learned about the requirements of such a device, what developments would have the most significant impact and how controlling coronal plane ankle behavior affects amputee stability. The purpose of this research is to describe the first step in this process – a proof of concept for a novel prosthetic ankle that can adjust the coronal plane stiffness in a controlled manner.

## 1.1 Balance for Amputees

For lower limb amputees, quality of life is directly related to the functionality of their prosthetic device. While each individual's case is different, studies have shown that more than half of amputees report some dissatisfaction with their lower limb prosthesis [1]. A significant area of improvement identified by amputees is in the mechanical functionality of the device [2]. This goes hand in hand with an amputee's confidence in the device that they are using. Balance confidence has been directly related to mobility and participation in social activity. In one study 49% of sampled amputees are reported to have a fear of falling which can have a direct detrimental effect on quality of life [3].

Uneven terrain can cause significant disturbances in gait and lead to balance problems. Amputees have much more variability in their medial-lateral stability than non-amputees while walking on uneven ground [4]. Actively avoiding uneven terrain directly affects the quality of life of an amputee. Improving the functionality of lower limb prostheses for traversing uneven terrain is therefore an important step in improving the quality of life of amputees.

## 1.2 Biological Aspects of Inversion and Eversion

When designing prosthetic devices, one thing to strive for is the functionality of the biological limb that the device is attempting to replicate. The multi-joint system between the lower leg and the foot allows for a complex range of motion. The main ankle joint consists of the tibia and fibula interacting with the superior surface of the talus and is responsible for the majority of motion in the sagittal plane for plantar and dorsi-flexion. This hinge like joint is referred to as the talocrural joint. Inversion and eversion primarily occur at the subtalar joint, where the distal end of the talus interacts with the calcaneus. Both joints contribute to inversion and eversion, just as both joints contribute to dorsi and platar-flexion. However, the contribution of the subtalar joint to inversion and eversion is more significant than that of the talocrural [5]. The axis of rotation for inversion and eversion is not fixed due to the interaction of multiple joint surfaces between the talus and the calcaneus in which both translations and rotations occur. Attempts to recreate the bone structure of this joint can perhaps best be seen by the complexity and changes in design of total ankle replacements [6].

Muscles and ligaments work together in an active and passive capacity to control the stability of the ankle. Six major ligaments and nine primary muscles control inversion and eversion. Between these muscles, ligaments and joint surfaces ankle position, stiffness and damping can be controlled. Ultimately, foot position is the most important property, but without investigating the active position control of the ankle, the foot position is mostly determined by the applied load and the stiffness of the ankle. In the coronal plane, therefore, one of the more important measures of the system is the stiffness. Stiffness of the ankle in the sagittal plane has been quantified in a number of ways with a number of tools [7-9]. Stiffness in the coronal plane has received less scrutiny. Those studies that have been done tend to focus on stiffness while standing still [10, 11]. Work has been done to fully model the kinematics of the human foot based on the shapes and material properties of bones, ligaments and tissues of the foot [12, 13] However, a thorough literature investigation did not find any research on coronal plane ankle behavior for level ground walking and walking on uneven terrain.

## 1.3 Existing Devices

Most lower limb prosthetic devices on the market focus on the functionality in the sagittal plane. This is only natural since one of the primary goals of a prosthetic ankle should be to assist in walking, an activity where the majority of the plantar and dorsi-flexion motion occurs in the sagittal plane. Some devices do have designed coronal plane properties allowing inversion and eversion. The following is a list of some of the commercially available foot and ankle systems that manufacturers claim are multi-axial:

- Earthwalk™ Ankle (WillowWood™, Mt. Sterling, OH)
- Seattle C-stance® Ankle (Model and Instrument Works, Seattle, WA)
- Multiflex Pyramid Ankle (Endolite, Miamisburg, OH)
- Elite2 (Endolite, Miamisburg, OH)
- Talux® (Össur, Reykjavik, Iceland)
- Renegade® AT (Freedom Innovations, Irvine, CA)
- WalkTek™ (Freedom Innovations, Irvine, CA)
- Trustep (College Park, Warren, MI)

There are two common methods for allowing multi-axial motion for inversion and eversion. The first is to rely on the shape of the foot or ankle to allow for deflection for inverting and everting. Generally this is done with a split keel foot as seen in the Freedom Innovations Renegade® and the Endolite Elite2. The Seattle C-stance ankle also allows for inversion and eversion through the deflection of the c-shaped carbon fiber spring.

The other primary method for adding inversion and eversion to a foot is to use a multi-axial joint with rubber bumpers that can deform medially and laterally. For example, the Endolite Multiflex Pyramid Ankle has a ball joint with a rubber ring bumper that controls the plantar and dorsi-flexion as well as the inversion and eversion. The Össur Talux and the Freedom Innovations WalkTech also use some form of rubber bumpers to control the displacement of the multi-axial system.

The main limitation to all of these devices is that they only allow for one stiffness setting at a time. Thicker material in the formed feet allows for changes in stiffness, but these discrete predetermined material characteristics are typically prescribed based on weight an activity levels. An individual with a particular style of foot would not have independent control of just the coronal stiffness. Changing rubber bumpers may not require a whole new device, but is still limited by the discrete, predetermined material characteristics of different rubbers that are again typically prescribed based on weight and activity.

Even by changing devices or rubber bumpers to increase or decrease stiffness, current devices do not allow for independently altering the coronal stiffness. Studying the effects of changing the stiffness in the coronal plane cannot be conducted without changing the stiffness in the sagittal plane. With these changes, it would be difficult to tell if altered gaits were due to the change in coronal plane properties or sagittal plane properties.

## 1.4 Need

Current lower limb prosthetic devices are very limited in their functionality when compared to the biological system that they are attempting to replace. This is especially true when characteristics in the coronal plane are considered. A limited body of knowledge for defining the optimal characteristics for a prosthetic device encountering uneven ground prevents significant improvements in manufacturer approaches to this issue. One need is therefore for more research in biological ankle properties, especially with regard to walking and walking on uneven terrain. This type of data would help to establish the characteristics that prosthesis designers should attempt to emulate.

Steps can be made from the current state of the art towards a more functional lower limb and perhaps total biological limb simulation is not necessary for vast improvements in amputee satisfaction and confidence. With medial-lateral stability identified as an important factor, more data needs to be collected to understand how changes in coronal plane properties might affect and ultimately improve amputee stability and therefore their quality of life.

The goal of this project is to design and construct a prosthetic ankle that is capable of controlling the rotational stiffness in the coronal plane. This device will be used to collect data and help determine how adjusting the coronal plane stiffness affects the stability of amputees.

# 2 Methods

A novel prosthetic ankle was designed that allows for the control of the coronal plane stiffness. This section includes a description of the ankle as well as experiments used to evaluate the capacity of the device. These validation tests consisted of both bench testing and human subject testing. The bench tests described include comparisons of the ankle capability with devices currently on the market as well as its adjustment speed and controllability. The human subject test was used to evaluate the functionality of the ankle as a prosthetic device as well as to collect initial data on amputee performance walking on a side slope with different stiffness values.

## 2.1 Device Description

The device described in the following sections was developed through an extensive process of investigating design requirements, functionality requirements, and feasibility. The device would need to be robust enough to withstand the loading due to walking. For a 100kg individual, this comes out to less than 2500N of applied force. Individual structural components were modeled with such loads in a basic finite element analysis using SolidWorks (Dassault Systèmes SolidWorks Corp., Waltham, MA). This had to be balanced with making it lightweight, defined as less than the limb that it was replacing, nominally 2kg, though the lighter, the better. Inversion and eversion range was determined to be 15 and 5 degrees respectively. The device also had to be independently powered.

A number of designs were considered that would allow for motion in the coronal plane including adjustable nozzle passive hydraulic systems, adjustable length coil springs and horizontal cantilever beams. The final design as described in the following section was chosen because of its simplicity and ease of manufacturing, ability to directly control the stiffness rather than damping as in the passive hydraulic system, and the low power requirements for changing the stiffness unlike pre-loading coil springs.

The requirements for spring stiffness values and control systems were less well understood. Rough estimates were initially made and modeled with room in the final design for adjusting these different characteristics, for example, using different spring dimensions. Ideally for the control, the device would be able to react to large moment inputs or follow a stiffness profile defined by the state of the gait cycle. The

driving mechanisms need to be able to adjust over a wide range of stiffness values in less than a second, approximately an average walking pace. However, for the scope of this first prototype, simply being able to adjust the stiffness to predetermined settings was sufficient with room to expand the control functionality.

### *Mechanical Design*

The Controlled Stiffness Ankle or CSA is shown in figure 1. The coronal rotation is simplified to a pin joint pivot. The bottom “foot” assembly rotates about the pivot. Two cantilever beam springs are fixed to the foot assembly parallel the upper “shank” assembly of the device when not loaded. A cart on the shank slides up and down the cantilever beam springs on a set of rollers. When a moment is applied to the ankle, the cart pushes on one beam and pulls on the other, deflecting the cantilever beams until the moment is equalized. Based on the length of the beam, the applied moment will cause a different amount of angular displacement about the pin joint. A shorter effective beam length is stiffer than a longer effective beam length. The position of the cart therefore determines the effective length of the spring.

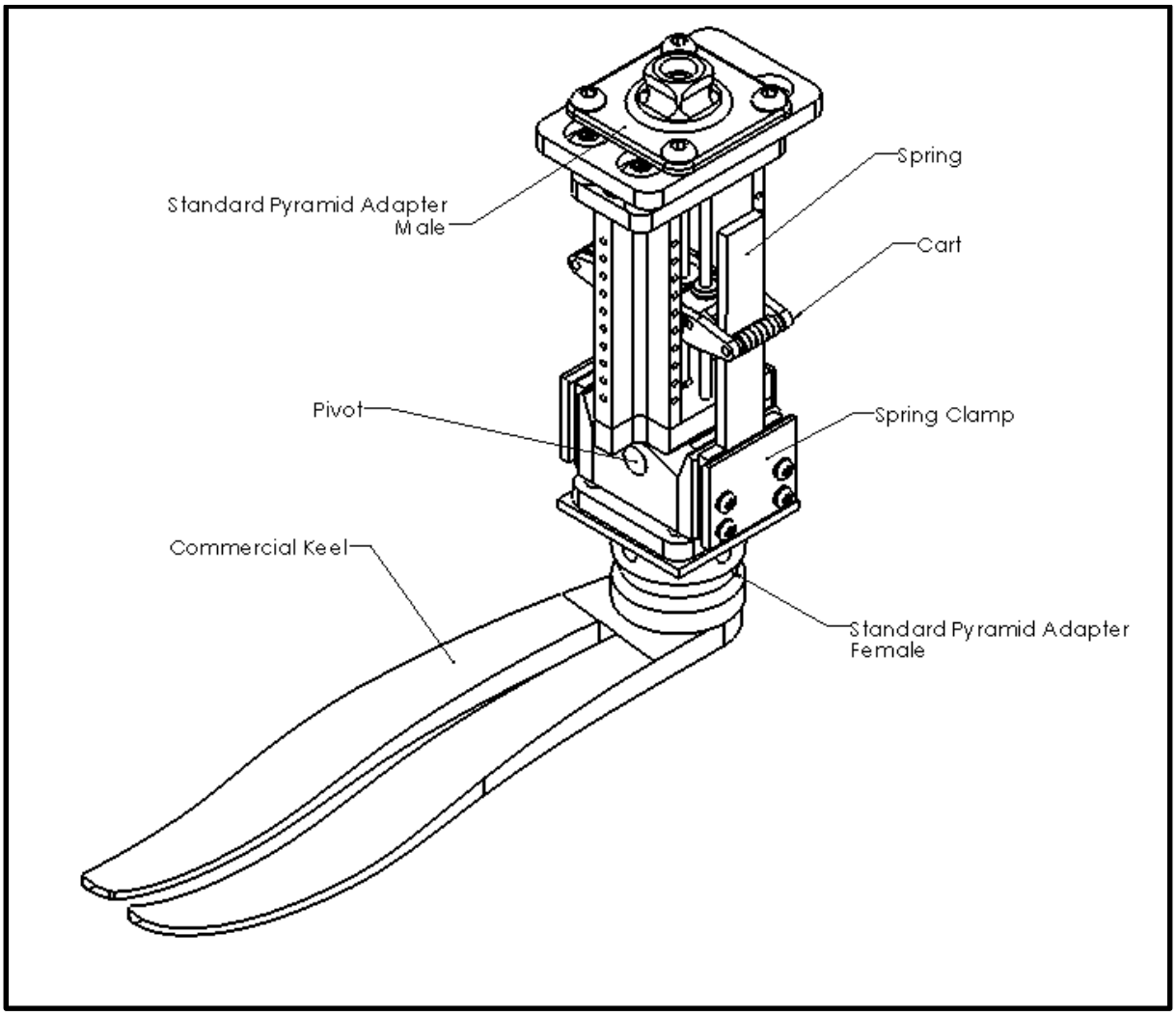


Figure 1: Controlled Stiffness Ankle (CSA) which rotates about the pivot when a moment is applied, deflecting the cantilever beam springs according to where the cart is positioned.

The cart moves up and down two rods via a stainless steel ACME screw and brass nut with a ¼-20 thread. The pitch of the thread prevents back-driving and thus the system only needs to be powered for changes in position and not maintaining positions. The screw is turned by a gear driven by a 30 Watt brushless motor (EC-16 #400160, Maxon Motors, Sachseln, Switzerland). The motor driving the screw, pushes the cart either up or down the cantilever beams, thus lengthening or shortening the effective length of the beam. Figure 2 shows how the spring deforms when a load is applied on a 15 degree everted plane when a particular spring set is at its most compliant position.

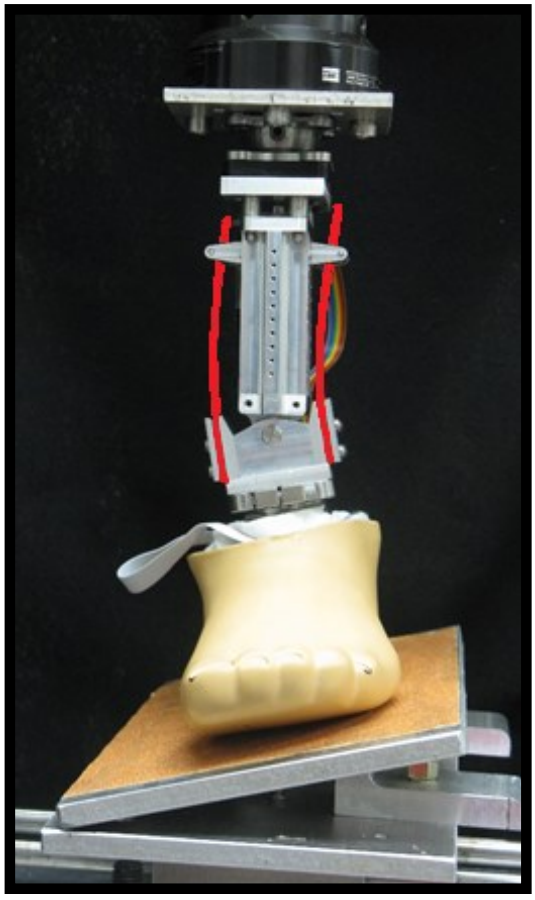

Figure 2: CSA with cosmesis on everted plane. Deflected beams are in the most compliant setting, highlighted in red.

The springs were designed to provide a wide range of possible spring thicknesses and a wide range of lengths for each spring option. The cart can accommodate spring materials up to 18.5mm wide, between 1.2 and 5.1mm thick. The minimum effective length of the spring is 14.8mm and the maximum effective length is 76.8mm with a total travel of 62mm.

The minimum stiffness is only limited by how thin the material can be without breaking. The maximum stiffness is only limited by the elastic modulus the material selected. For the purpose of initial testing with this device, the material chosen was a carbon fiber laminate (#8194K12, 8194K14, 8194K16, McMaster-Carr, Los Angeles, CA). Different sets of springs were made including pieces 0.79mm (1/32in), 1.59mm

(1/16in) and 3.18mm (1/8”) thick pieces all 16.5mm (0.65in) wide. Each piece was cut to be long enough to be securely clamped and cover the full range of motion of the cart.

The frame of the device was designed to allow for clamping the spring, attaching standard pyramid adapters to either end, constraining the movements of the cart to linear displacement along one axis, constraining movement of the joint to rotation about the pin and allowing for the attachment of electronics, sensors and control systems. The main structure of the frame was designed to withstand the forces of walking with an adequate safety margin. This was generally based on the International Test Standard loading specifications outlined in ISO 10328.

The overall weight of the mechanical components of the device including the motor is 675g. With electronics and batteries, it weighs 1120g. This is an additional 1120g to what the standard foot and pylon system would otherwise weigh. The length of the device is 170mm. This requires a clearance between foot and socket adapters of an equal or greater distance.

### *Electrical and Control Design*

The minimal electronics for this system include a means of programming the input to control the position of the cart, or effectively the number of turns of the motor. Figure 3 outlines the system consists of a brushless motor, an encoder, a master micro controller, a slave micro controller, a motor controller, a digital to analog signal converter, an encoder counter chip. The controls are powered by a 7.4V lithium battery (Tenergy, Fremont, CA).

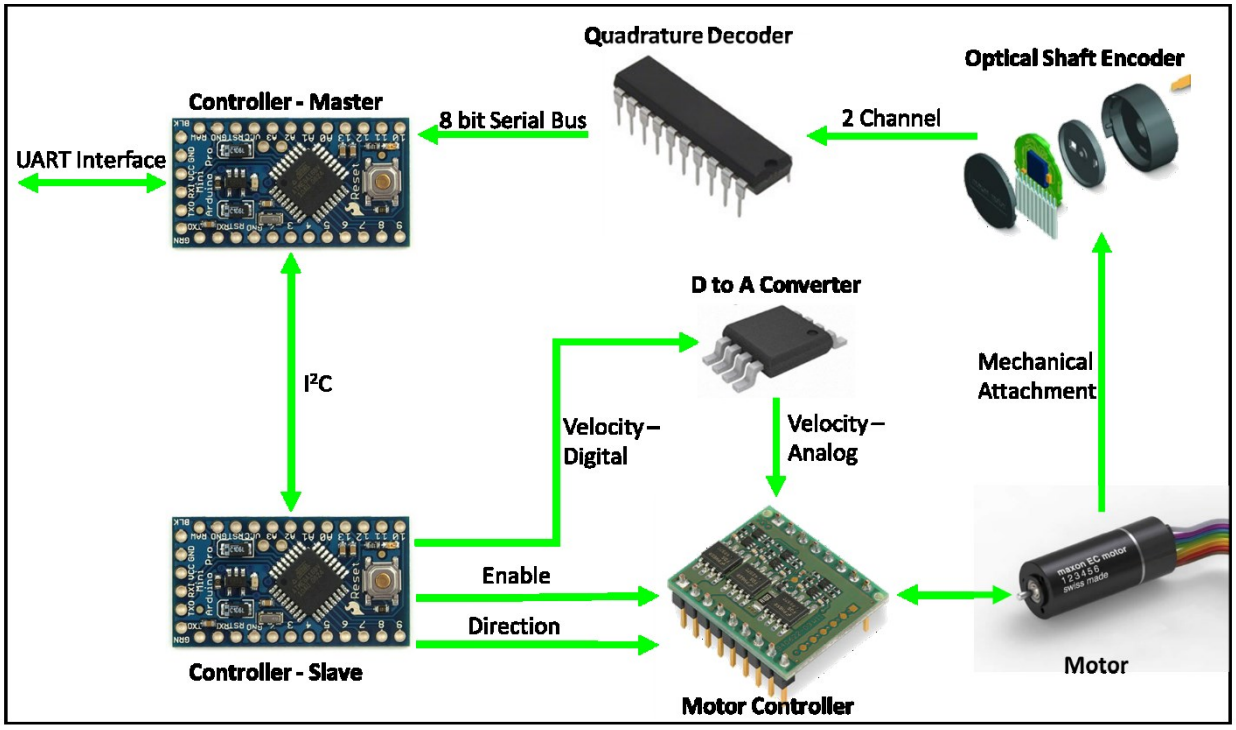


Figure 3: Electronic position control communication diagram.

The motor is speed controlled using the motor controller (367661, Maxon Motors). The motor controller has two power inputs, the controller power with a regulated 5VDC coming from the master micro controller (Arduino Pro Mini, Sparkfun, Boulder, CO) and the motor power coming from the 14.8V lithium battery (Tenergy). The control loop of the motor controller is a PI loop pre-programmed on the motor controller chip. This uses input from the Hall effect sensors of the motor. With standard speed range and current limits, the only user controlled inputs are the enable switch, the direction switch and the speed selection signal. The enable and direction are simple binary signals controlled by the slave micro-controller. The speed select signal is an analog voltage between 0 and 5V produced by the digital to analog signal converter (MCP4921T, Microchip, Chandler, AZ). The DAC receives a PWM signal from the slave micro-controller (Arduino Pro Mini, Sparkfun). This allows for a range of 0-5V divided into 1024 increments.

The quadrature encoder (228181, Maxon Motors) installed in line with the motor has 1024 counts per revolution of the motor. At this rate with the maximum speed of the motor at approximately 40k rpm, the encoder counting is much too fast for the micro-controllers to handle. Therefore, an encoder decoder

counting chip (HCTL-2022, Avago Technologies US Inc., San Jose, CA) is installed such that the counts of the motor are incremented or decremented as necessary and the value is stored on the chip. The master micro-controller can poll this chip whenever necessary and receives a 32-bit integer indicating the count of the encoder at the time of the poll request. This is transferred via an 8-bit bus to the micro-controller.

The final control package with batteries attached to the device can be seen in figure 4.

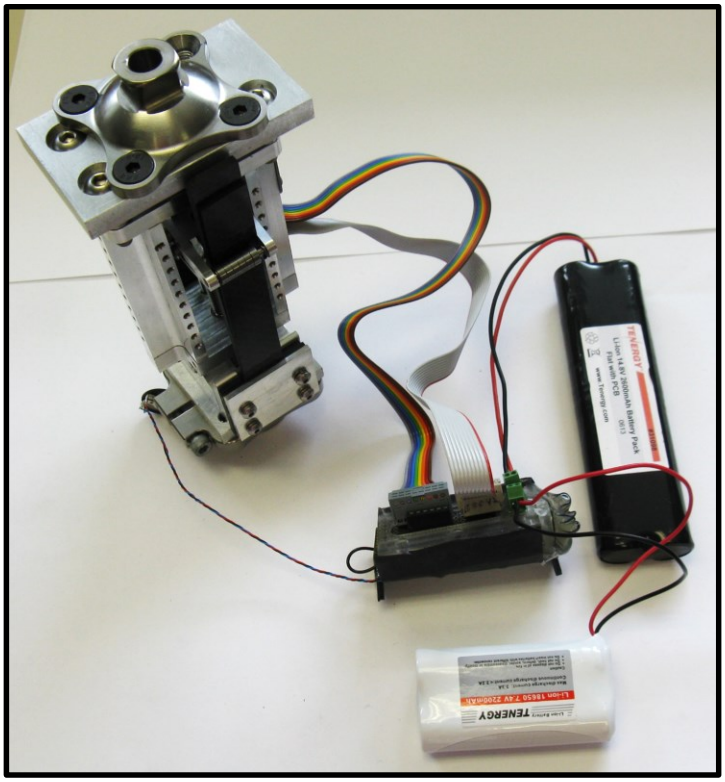

Figure 4: CSA with controller and batteries

For the scope of this project, the control system is only concerned with timing the change in position of the cart. Two different methods were used. The first was a simple open-loop system concerned with only the absolute position of the cart simply requiring only predetermined positions to be reached. The motor is simply powered to maximum speed until a certain threshold within the target destination is reached, at which point power is cut to the motor and the system stops within a previously evaluated distance. This is effective for gross movements, but loading and the distance traveled directly affect the “coasting” time after the power is cut. This error could be as much as 0.063” from the intended position.

A second control system for the cart position is concerned with position profiles. The simplest profile is defined by how many turns are needed and the amount of time to perform the turns. A velocity profile is then generated including an acceleration phase, maximum velocity phase and a deceleration phase with the maximum values for acceleration, deceleration and velocity limiting the profile. Using the internal timing unit of the micro-controller and the encoder count, a simple PI loop is used for matching the predetermined velocity. Position samples can be taken at approximately 250Hz while data is being logged – faster if no external communication is taking place. The velocity can be calculated and compared to the expected velocity. The 'P' is based on the velocity error and the 'I' is based on the position error. With these two factors, the correction value can be calculated and used to adjust the motor controller velocity signal. This is easily expanded to more complex profiles, requiring only a definition of the desired velocities at any given time.

On the axis of rotation for the ankle, a potentiometer is used for gross angular measurements. For the scope of this project, the potentiometer input is not utilized. Other inputs are included on the device package for future sensor expansion. This includes regulated 5VDC, two analog I/O signals, two interrupt signals that can be used as 5V digital I/O and one other digital I/O.

A more detailed design description is given in Apendix A.

## 2.2 Bench Testing

During development of the device, a number of bench tests were used to identify empirically certain characteristics and to evaluate functionality. In this case, the stiffness of the springs at different cart positions was defined empirically. Evaluation included a comparison with existing prosthetic feet and performance testing of the drive system. Characterizing the spring stiffness values was important to use in any future experimental analysis of ankle stiffness relative to balance and to establish the relation between the effective spring length and the stiffness of the system. The commercial device comparison was used for the purpose of demonstrating how the CSA would be able to replicate a range of stiffness values exceeding a range of commercial stiffness values.

*Spring Characterization*

The first bench test was used to determine the relationship between cart position and angular stiffness of the ankle. In order to program the device for a specific angular stiffness, it is necessary to know what the stiffness is at any given cart position. While this can be estimated with a complex model of the system, it is more efficient to simply empirically derive the relation. This was done using an MTS testing machine (MTS, Eden Prairie, MN), recording displacements and forces. The ankle was fixtured horizontally such that the vertical piston of the MTS pushed down on the "top" of the ankle, deflecting the shank of the device around the pin joint as seen in Figure 5.

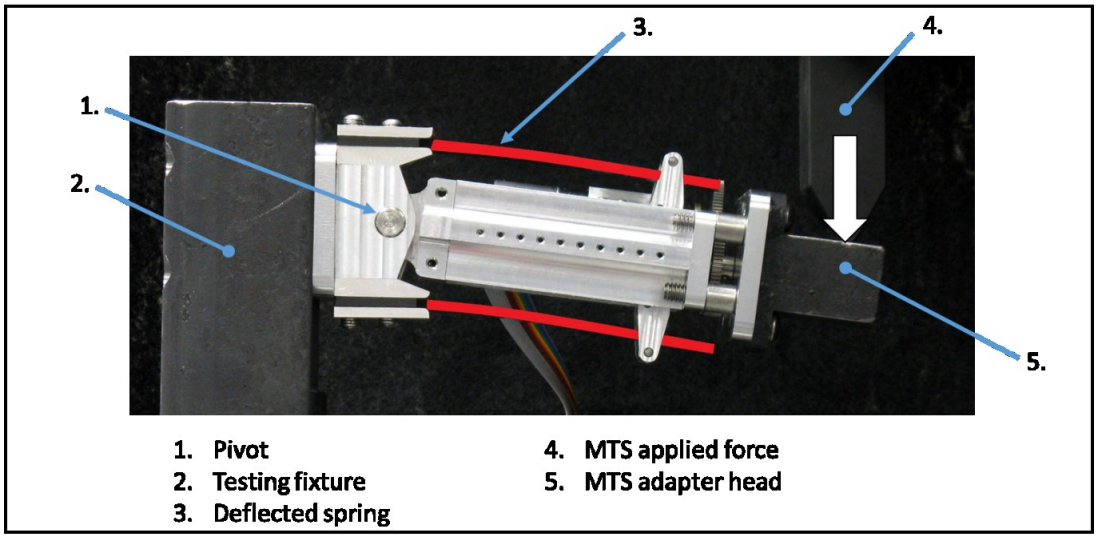


Figure 5: Spring characterization test with springs highlighted in red to show deflection.

This was done with cyclic loading to a displacement of 15mm at 0.3 Hz for 30 cycles at each position. Data points were recorded at 99 Hz. Data collection started with the cart in the most compliant position. After the first set of data for 30 cycles was collected, the cart was moved to a stiffer position by two rotations of the ACME screw, moving the position of the cart 0.1 inches. Data was collected for 24 positions, between the most compliant setting and 2.4 inches down the spring – 61mm of the total 62mm range of motion. For each setting, the slope of the displacement to force relation of the data points was calculated. Each setting was very linear and the slopes were recorded. For each spring set, these stiffness values were plotted against the position of the cart. Thus the relation between the cart position and the angular stiffness for four spring set combinations was plotted to characterize each spring set. The spring sets that were tested can

be seen in figure 6. These different spring sets will be referred to throughout this paper by this numbering scheme.

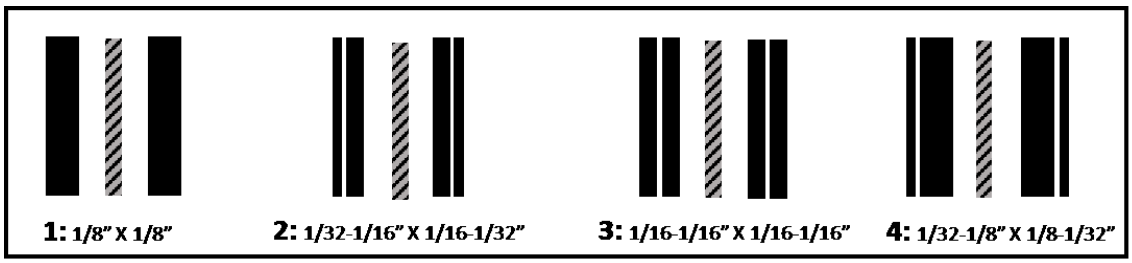


Figure 6: Tested spring combinations. This represents a stylized anterior view of the device. The black rectangles represent the relative thickness and position of the spring material while the cross hatching represents the ACME screw between the springs. The notation indicates the order of the spring material. Spring sets will henceforth be referred to by these numbers.

## *Commercial Device Comparison*

The next bench test concerned comparing the stiffness of the device when attached to a prosthetic foot to the stiffness of a few different commercial prosthetic feet. The purpose of this test was to evaluate if the ankle could be used for such tests where a researcher could alter the coronal stiffness of the ankle over a range of values represented by different types of feet. This would allow for stiffness comparisons without having to switch feet and would allow for a much greater range of variability, only changing the variable of coronal stiffness. Ideally, this comparison also shows that the CSA has a much wider stiffness range than an array of commercial devices.

The MTS was set up with a female pyramid adapter on the upper piston. An X-Y stage was attached to the lower piston, generally centered but providing a means of fine tuning the position of the fixture. The sliding friction plate was then attached to the stage. This plate included a fifteen degree slope covered in sand paper that was able to slide medially and laterally on linear bearings. The sandpaper kept the cosmesis from sliding on the inclined plane. Initial tests were conducted with a fixed plate, but it soon became apparent that the system was over defined for ankle rotation and the sliding friction plate setup was developed, similar to previously defined methods of evaluating inversion and eversion limits [14]. By changing the orientation of the plate, 15 degrees of inversion could become 15 degrees of eversion. A sample foot with a cosmesis was attached to the upper pyramid adapter. The setup is shown in figure 7.

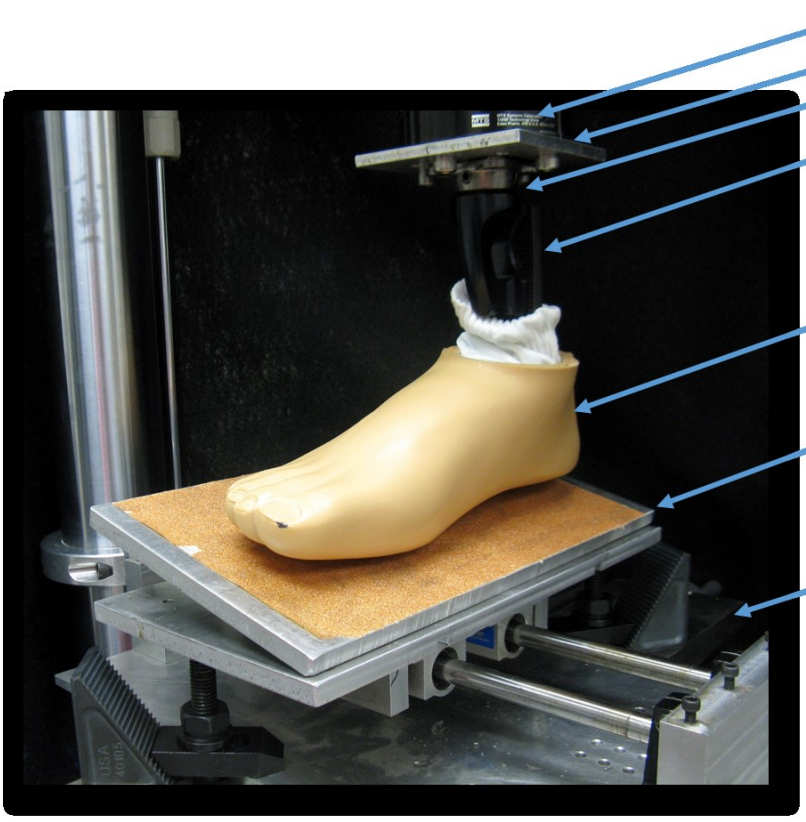


Figure 7: Inversion and eversion foot comparison bench test setup.

The feet used in the test were the Össur Vari-Flex with Evo in both category 5 and category 8 stiffness, the Össur Low Profile Vari-Flex in category 9 and the Freedom Innovations Sierra in categories 4 and 8. All the feet tested were right feet, except the LP Vari-Flex was a left. All tests were done with a liner sock and a cosmesis and without any shoe. The heel of the foot was positioned to be the manufacturer recommended height.

The foot was positioned directly over the plate. The plate was slid such that the foot made contact with the plate. The system was then zeroed for both force and position. The foot was then loaded to approximately 50 Newtons. The system was zeroed again. Using this origin point under load meant that returning to “zero”

would keep the foot loaded and prevent the plate from slipping in relation to the foot. The foot was then loaded to approximately 500-600 N. The displacement was noted as the maximum displacement for the cycle.

The MTS was then programmed to cycle the position of the foot from the initial 50 N to the noted maximum position using position control. The foot was not fully unloaded to prevent the sliding friction plate from slipping in relation to the foot. This cycle was repeated 50 times at 0.5 Hz. Force, position and time data was recorded for this period at 99 Hz. Based on the standard minimum sample frequency of ten times the cycle frequency, this was doubled due to the low number of cycles. The 99Hz was chosen so as not to be an even fraction of 0.5Hz within the 50 samples, thus creating a smoother line of data points.

Each foot was tested in both inversion and eversion. For the CSA, two different spring setups were used based on data collected previously. Each CSA spring combination was tested at the most stiff position, the least stiff position, and the middle position as shown in figure 8. The middle position was defined as the cart being positioned halfway between the stiffest position and the most compliant position. In figure 8 the cantilever beam springs have been highlighted in red to show displacement. The white arrow represents the direction of the applied force during loading. The green arrows represent the applied forces on the cantilever springs.

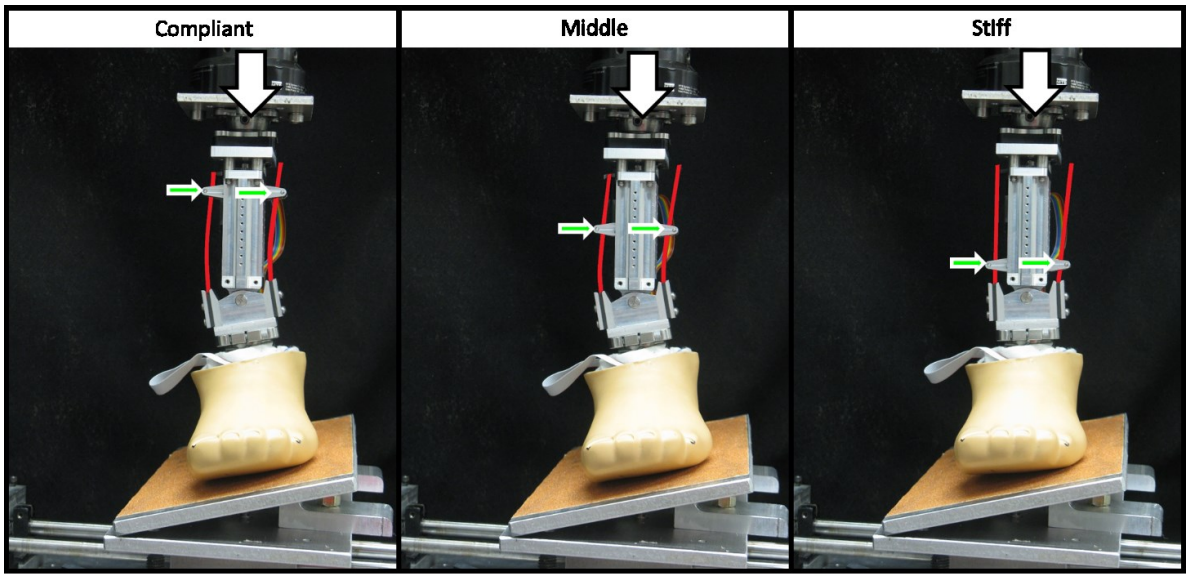


Figure 8: Eversion foot test with the CSA springs set to three different stiffness values under the same loading condition. The vertical white arrow represents the direction of the loading force. The small green arrows represent the direction of the forces being applied to the springs. The springs are highlighted in red.

The systems that were tested are shown in table 1. Each setup was tested in both inversion and eversion for a total of 20 data sets of 50 cycles each.

Table 1: Devices tested for inversion and eversion stiffness characteristics on MTS

| Foot | Category | Spring | Position |
|---|---|---|---|
| **Össur Vari-Flex® with EVO™** | Cat. 5 | - | - |
| **Össur Vari-Flex® with EVO™** | Cat. 8 | - | - |
| **Freedom Innovations Sierre®** | Cat. 4 | - | - |
| **Freedom Innovations Sierre®** | Cat. 8 | - | - |
| **Össur Vari-Flex® Low Profile** | Cat. 9 | #3 | Stiff |
| **Össur Vari-Flex® Low Profile** | Cat. 9 | #3 | Middle |
| **Össur Vari-Flex® Low Profile** | Cat. 9 | #3 | Compliant |
| **Össur Vari-Flex® Low Profile** | Cat. 9 | #1 | Stiff |
| **Össur Vari-Flex® Low Profile** | Cat. 9 | #1 | Middle |
| **Össur Vari-Flex® Low Profile** | Cat. 9 | #1 | Compliant |

The categories shown in table 1 are generally defined as what different manufacturers believe is appropriate for different body weight and activity levels. While the weight and activity categories are consistently defined, the mechanics of the devices vary according to different manufacturers.

One note is that the CSA with the #3 springs at the most compliant position was too compliant for fully loading to 500N. The device risked reaching the hard-stop angular limits of 20 degrees either direction. To prevent this from occurring, these conditions were only tested to approximately 225N.

The data collected was then post processed. This included eliminating the beginning and end of each sample, leaving the middle 40 cycles to eliminate any end condition artifacts in the data. The remaining data points were then divided into loading and unloading. For the scope of this study, only the loading conditions were compared. Data points comparing displacement to force were then plotted as described in the results section.

### *Cart Position Control Characterization*

The first step to cart position control characterization was to ensure that the cart could move the required range of the device while loaded. After evaluation of movement, control characterization could be done including: speed, accuracy and repeatability.

Initially, eight different position control tests were planned with two different distances and four loading conditions. The longer distance was a change of 38mm or approximately 63% of the total range of the device. The shorter distance was a change of 13mm or approximately 20% of the total length. These lengths were chosen as a representation of the potential range that the cart might have to move to replicate the range of stiffness values encountered in commercial devices. The four loading conditions included unloaded, loaded vertically to 1000N, loaded on a fifteen degree inverted plane to 1000N and loaded on a 15 degree everted plane to 1000N. Table 2 shows the eight tests that were planned.

Table 2: Motor load testing conditions.

| Trial | Distance | Load Condition |
|---|---|---|
| 1 | 0.5 in | Unloaded |
| 2 | 0.5 in | Vertical Load – 1000N |
| 3 | 0.5 in | 15° Inversion – 1000N |
| 4 | 0.5 in | 15° Eversion – 1000N |
| 5 | 1.5 in | Unloaded |
| 6 | 1.5 in | Vertical Load – 1000N |
| 7 | 1.5 in | 15° Inversion – 1000N |
| 8 | 1.5 in | 15° Eversion – 1000N |

The loading was done with the MTS. For the inverted and everted conditions, the angled sliding friction plate was used as it was in the commercial device comparison test. The foot used for this test was an Össur Vari-Flex Low Profile, category 9. The springs used was the #1 spring set.

The motor was given a position control loop in which the motor was given a full power signal until a certain position marker was noted with the encoder. At this point the motor would reverse signals to full power the opposite direction until a similar position marker was reached according to the encoder output. After a one second pause, the cycle was repeated. This was repeated at least three times for each condition.

Encoder position and timer data was streamed from the controller to a computer via a UART serial connection (PuTTY 0.62) into a data log file. The data log file could then be evaluated for position, velocity, position accuracy and precision.

Data was collected for the unloaded and the vertically loaded condition. Unfortunately, the motor could not move the cart for the inverted or the everted conditions when loaded to 1000N and data was therefore not collected for these conditions. This was most likely due to the excessive deflection of the guide rods and the ACME screw. Any significant deflection in either of these components greatly increases the friction of the system. In this case, such an increase was sufficient to prevent the cart from moving.

For the data that was collected, the average time to travel the specified distance and back was evaluated and compared as described in the results section.

## 2.3 Human Subject Testing

The human subject tests were used to quantify some aspects of how this ankle would be used to further understanding and research about stiffness in the coronal plane. The first test was done to evaluate stability using a stationary standing balance test. The second test was to evaluate rotational stiffness during the gait cycle.

### *Standing Balance Test*

The purpose of the standing balance test was to see if the stiffness of the ankle in the coronal plane would have any significant impact on quiet stance stability. This was tested with one subject in five conditions: three stiffness conditions of the CSA, a rigid pylon with the same foot, and the prescribed device of the subject. A number of methods have been described for measuring standing balance [15-17]. For the purpose of this test, the center of pressure (CoP) position was measured using a force plate (Kistler 9286AA

portable force plate, Amherst, MA) From this data the CoP velocity and position standard deviation could be determined.

The subject signed an IRB approved informed consent form. Five conditions were tested, the first three using the CSA with the #1 carbon fiber laminate springs attached to a size 27 Vari-Flex® Low Profile category 9 prosthetic foot and cosmesis. The subject's prescribed foot was a Vari-Flex® category 5. The subject wore a pair of modified walking shoes (MW577, New Balance Athletic Shoe, Boston, MA).

Before each test, the subject had 15-30 minutes to become accustom to the foot and ankle combination that was tested. The subject stood on a force plate with feet placed together. For the duration of each test the subject was instructed to keep feet together with hands at the sides, eyes closed and try to maintain an equal distribution of weight on both limbs while standing as still as possible. The setup is shown in figure 9. CoP position data was collected at 1200 Hz for one minute.

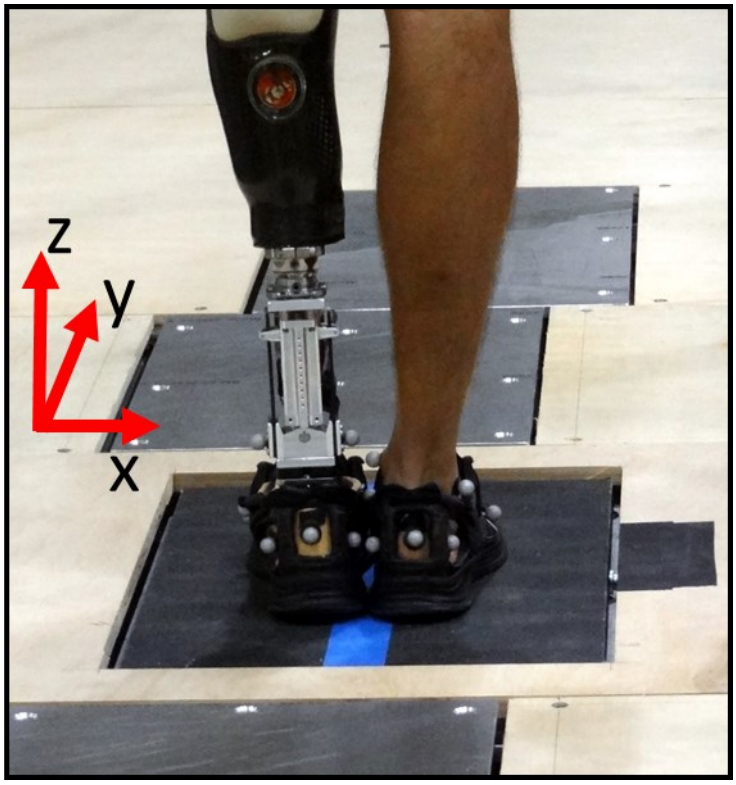


Figure 9: Standing balance test setup and coordinate system.

An initial trial was used to accustom the subject to the testing protocol. After more than 15 minutes of other walking activities, the first data collection was made. Each subsequent data collection occurred after a

period of 15-30 minutes of acclimatization on each new foot and ankle combination. The five conditions tested are shown in table 3.

Table 3: Tested conditions for standing balance test.

| Test | Condition |
|---|---|
| 1: CSA-C | CSA w/ Vari-Flex cat. 9 – Compliant |
| 2: CSA-M | CSA w/ Vari-Flex cat. 9 – Moderate |
| 3: CSA-S | CSA w/ Vari-Flex cat. 9 – Stiff |
| 4: RP | Vari-Flex cat. 9 – rigid pylon |
| 5: RX | Vari-Flex cat. 5 – prescribed device |

Each data set was trimmed to eliminate the first and last ten seconds of each trial to eliminate the beginning and ending data artifacts [16]. This data was then evaluated as the x-y coordinates of the CoP for each point in time. The metrics calculated were the overall range of displacement, the standard deviation of the displacement and the velocity. Each value was calculated independently for the x and y components to help distinguish between sagittal plane and coronal plane movements. The metrics and equations can be seen in table 4.

Table 4: Calculated values for standing balance test comparisons.

| Metric | Description |
|---|---|
| Range | $X_{max} - X_{min},\ Y_{max} - Y_{min}$ |
| Standard Deviation | $\sqrt{\frac{1}{N}\sum(x_i - \mu_x)^2}, \sqrt{\frac{1}{N}\sum\left(y_i - \mu_y\right)^2}$ |
| Average velocity | $\frac{1}{N}\sum\frac{x_i - x_{i-1}}{t_i - t_{i-1}}, \frac{1}{N}\sum\frac{y_i - y_{i-1}}{t_i - t_{i-1}}$ |

### *Walking on Uneven Terrain*

The purpose of the uneven terrain test was to see how the CSA responded to inverted and everted planes through an actual gait cycle. This test allowed for the quantification of rotational stiffness of the device and a direct comparison of different settings on the device, a rigid pylon and the subject's prescribed foot. This test also allowed for initial verbal feedback from the subject on stiffness preferences for handling uneven terrain, a topic that has not previously been able to be readily evaluated in a controlled manner.

The subject signed an IRB approved consent form. The test took place on a raised platform with five force plates positioned for five foot strikes over the course of the walkway as shown in figure 10 (4 AMTI 40x60 cm, Watertown, MA; 1 Kistler 9286AA portable force plate, Amherst, MA). The center force plate can be inverted or everted 15 degrees or left flush with the platform as shown in figure 11.

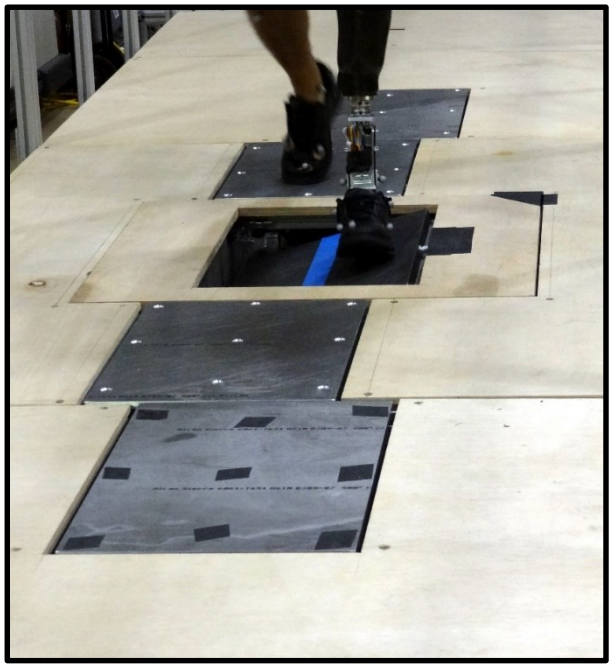

Figure 10: Subject walking across raised platform with five total force plates.

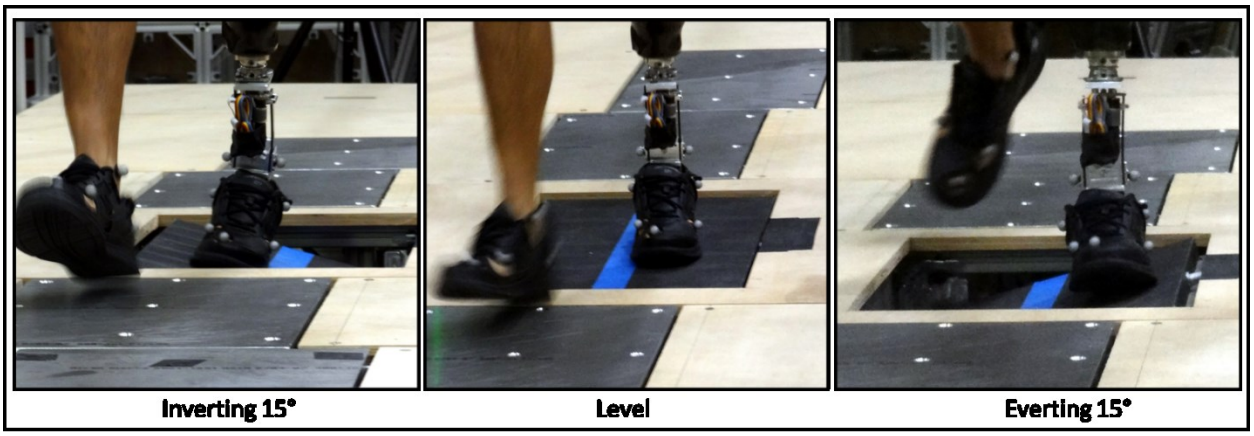


Figure 11: Different positions of uneven terrain force plate.

A full motion capture system (12-camera Vicon MX system, Vicon, Centennial, CO) was used with 67 total markers. Twenty-nine relfective markers were placed on the hands, arms, head, trunk, legs and feet according to the Plug-In-Gait full-body model (Vicon, Oxford Metrics, Centennial, CO) with a number of modifications. Clusters of four markers on a semi-rigid base replaced thigh wands and were placed bilaterally on the upper arm to minimize skin movement artifacts. Markers were also placed on the medial femoral condyles, tibial tuberosity, fibular head, and medial epicondyles to establish limb orientations. Toe markers were replaced with a marker on each hallux. Five additional markers were placed on the foot to define three separate segments of the Simplified Heidelberg Foot Model [18]. These include the hindfoot (lateral and medial calcaneus), forefoot (first and fifth metatasals) and hallux (toe). Two additional markers were placed to identify the location of the CSA axis of rotation. The subject wore modified walking shoes (MW577, New Balance Athletic Shoe, Boston, MA) with cutouts that would allow for the foot markers to be placed directly on the skin or cosmesis as seen in figure 12. Biometric measurements and modeling assumptions were made according to standard methods [19].

Figure 12: CSA and prosthetic foot in shoe with cutouts for mounting reflectors.

Five different conditions were tested. The CSA with a Vari-Flex Low Profile foot (Category 9, Ossur Americas, Aliso Viejo, CA) used the #1 spring set and was tested at the most compliant, stiffest and middle stiffness positions. A rigid pylon with the same foot was also tested. Finally, the subject's prescribed foot was used, a Vari-Flex Category 5.

A total of 75 trials were conducted including five trials of each of the following foot and ankle combinations and platform positions shown in table 5.

Table 5: Conditions tested for walking on uneven terrain.

| | **Plate Position** | | |
|---|---|---|---|
| **Foot** | Inverted 15° | Flat | Everted 15° |
| CSA – Compliant | CSA-C-I | CSA-C-F | CSA-C-E |
| CSA – Moderate | CSA-M-I | CSA-M-F | CSA-M-E |
| CSA – Stiff | CSA-S-I | CSA-S-F | CSA-S-E |
| Rigid Pylon | RP-I | RP-F | RP-E |
| Prescribed | RX-I | RX-F | RX-E |

For each combination, the subject was given 5-10 minutes to acclimate to the device. The subject then walked from one end of the platform to the other at a self-selected speed. Only trials with clean foot strikes on the force plates were included in the analysis. Five trials were performed for each foot and plate orientation combination.

Data was processed using a 15-segment whole body model in Visual 3D (C-Motion Inc., Germantown, MD). Three dimensional kinematics and kinetics were calculated for each trial using standard inverse dynamics techniques [20]. The metrics evaluated were the coronal plane angles and moments during stance of the ankle, knee and hip.

# 3 Results

## 3.1 Bench Testing

### *Spring Characterization*

The springs showed a predictable change in stiffness based on their effective length. As expected, the stiffness increased as the springs became shorter. Also predictable was the fact that the thicker material combinations were relatively stiffer for the same spring length. For example, spring #2 (as defined in figure 6) had a total spring material thickness of 4.75mm and spring #4 had a total thickness of 7.94mm. At the most compliant position, spring #4 was approximately 550% stiffer than spring #2.

Another interesting point was the difference between single springs and combined springs of the same thickness. While #1 had one 3.18mm spring on each side, #3 had two 1.59mm springs on each side. Combined, they had the same cross sectional area, however the stacked spring stiffness was significantly less. This also makes sense based on the simplified equation of the deflection of a cantilever beam where $\delta_x$ is the deflection, $F$ is the applied point load, $L$ is the distance from the fixed end to the point load, $E$ is the elastic modulus and $I$ is the area moment of inertia:

$$\delta_x = \frac{FL^3}{3EI}$$

The only difference between the two would be the area moment of inertia values.

$$I_1 = \frac{16.5mm * (3.18mm)^3}{12} = 44.22mm^4$$

$$I_3 = \frac{16.5mm * (1.59mm)^3}{12} * 2 = 11.05mm^4$$

This shows that even with the same cross sectional area, the moment of inertia was different. While the simplified, small displacement cantilever beam model indicates a difference of about four times, the real value changed over the length of the beam with the more compliant stiffness different by a factor of 3.9 times and the stiffer values different by a factor of 2.0 times.

Material limitations were also noted with springs that were too thin for the loading. The 1.6mm material of the #2 combination delaminated during the loading cycle 44 turns from the top. (Note: valid data was not collected for #3 between the top and 9 revolutions.)

These spring characteristics can be noted in figure 13.

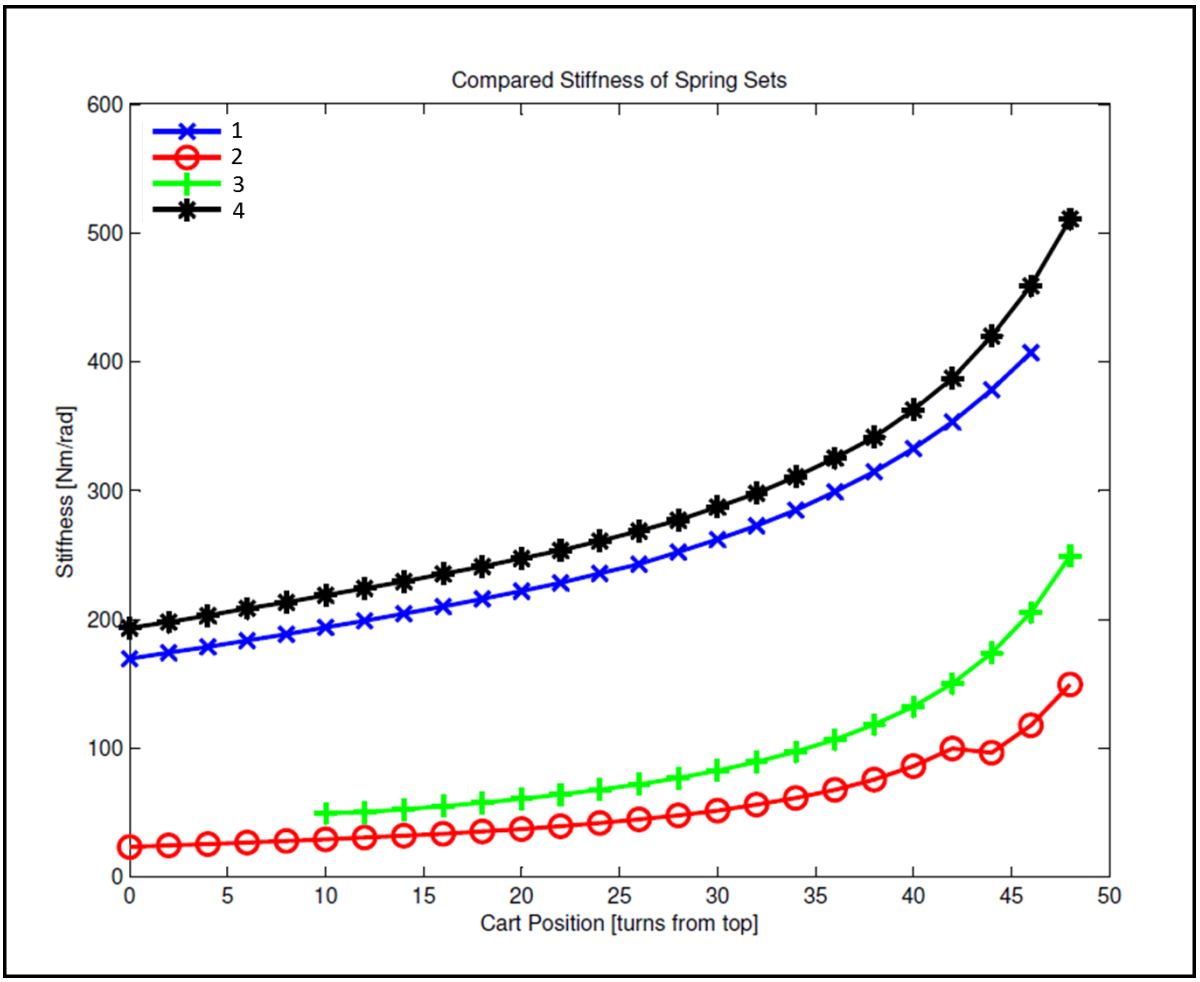


Figure 13: Angular stiffness values relative to cart position for four tested spring combinations.

## *Commercial Device Comparison*

The comparison of commercial prosthetic devices to the CSA included 20 different test – four commercial feet and two spring sets at three different positions, each in inversion and eversion. The resulting data was displayed as a vertical displacement in relation to the applied force with negative values indicating both a downward applied force and a downward displacement. While not directly comparable to stiffness values

reported as Nm/rad, these values are comparable between themselves and show the general relation of stiffness across the devices. Plotted data showed a different stiffness plot for loading and unloading, indicating hysteresis as seen in figure 14.

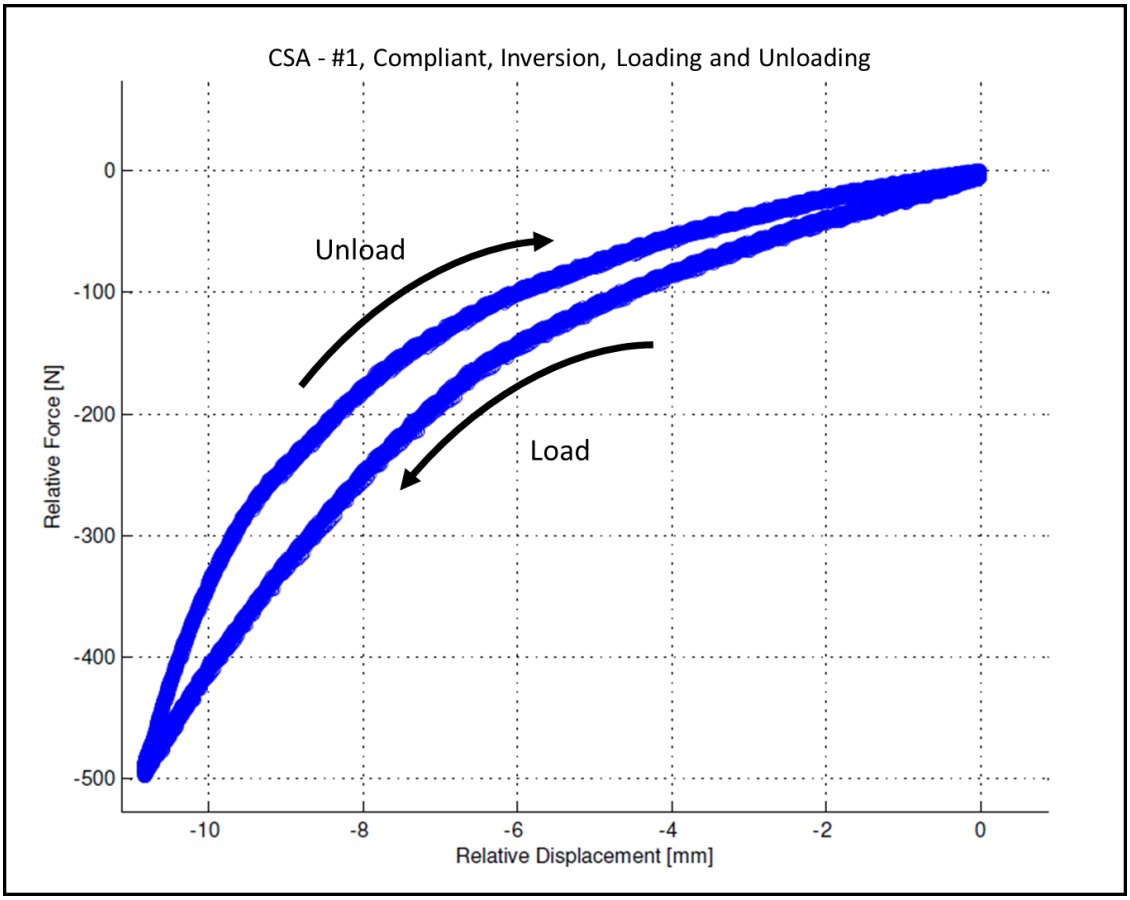


Figure 14: Relative stiffness of #1 spring set during loading and unloading.

The loss of energy, the area between the loading and unloading curves, was calculated for a few combinations to show the difference the difference between the hysteresis of the commercial feet and CSA. These values were calculated for the inversion conditions between 0N of loading and 500N and are shown in table 6.

Table 6: Energy loss due to spring hysteresis characteristics.

| **Foot and Spring** | **Energy Loss [mJ], [%]** |
|---|---|
| Össur Vari-Flex, cat. 5 | 293, 9% |
| Össur Vari-Flex, cat. 8 | 324, 11% |
| Freedom Innovations Sierre, cat. 4 | 359, 13% |
| Freedom Innovations Sierre, cat. 8 | 346, 12% |
| CSA #1 Spring, Compliant | 444, 12% |
| CSA #1 Spring, Stiff | 354, 13% |
| CSA #3 Spring, Stiff | 468, 14% |

In this case, the CSA with spring set #1 at 12.5 ±.5% energy loss was comparable to the commercial feet at 11.3±1.5%. The CSA with #3 springs was only slightly more inefficient, though this inefficiency is most likely due to the sliding friction between the stacked beams that are clamped together.

For simplifying comparison, only the loading condition was considered for further investigation. For the CSA, the top cart position proved to be the most compliant, the bottom cart position stiffest and the middle position had a stiffness value between the others as seen in figure 15.

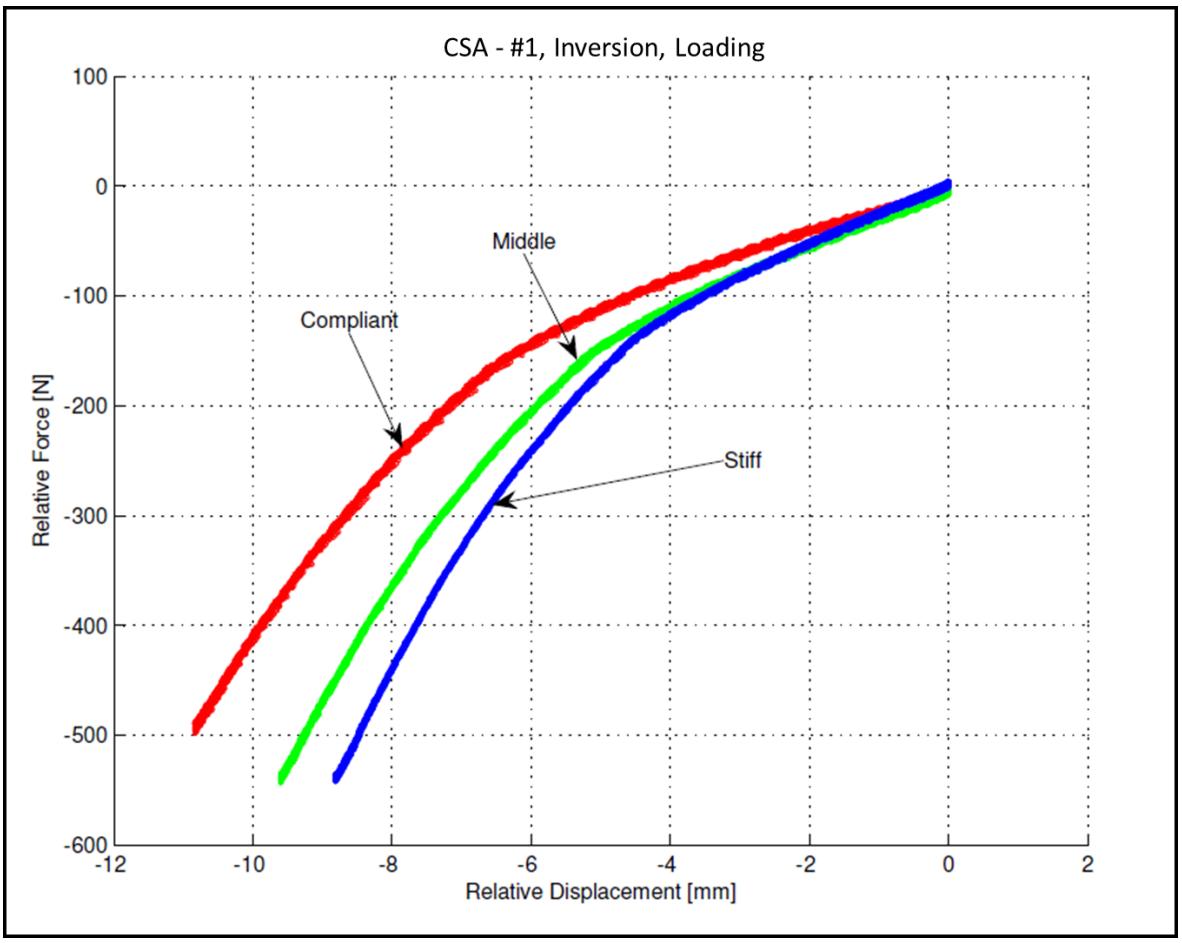


Figure 15: Comparison of three stiffness settings for the same spring set under just loading conditions.

Comparing the different devices simply requires comparing the displacement for a particular loading. For the CSA with a particular spring set to be able to replicate the stiffness of a commercial device, the commercial device displacement must be between the compliant displacement and the stiff displacement for the same loading. For example, the Össur Vari-Flex categories 5 and 8 stiffness curves fall between the stiffness curves of the CSA with the #1 spring set between the stiff curve and the compliant curve as seen in figure 16.

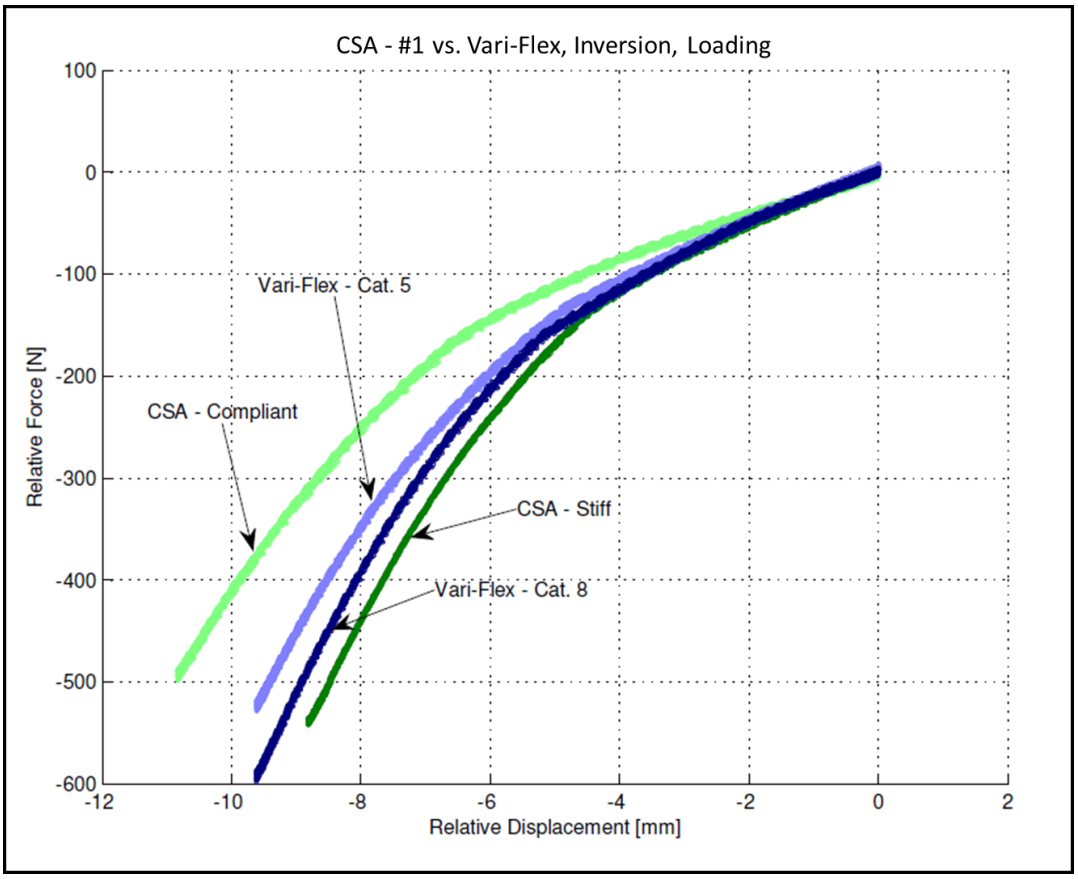


Figure 16: Comparison of range of a single spring set with the CSA to a range of categories of Vari-Flex feet.

The #3 spring set was shown to be significantly more compliant than the commercial devices and so the #1 spring set was used as the comparison. To simplify the comparison, three different loading values were chosen: 100N, 300N and 500N. At these different loading values, devices were determined to either fall within the range of displacement values of the CSA with #1 springs or not. Table 7 shows these values, highlighting which values met the criteria and which did not. The yellow cells of the table indicate the CSA with #1 springs to which the other values are compared. The green cells indicate values that fell within the CSA's range and red cells indicate values that did not.

Table 7: Evaluation of stiffness value ranges relative to the CSA with #1 springs. Yellow highlights the #1 spring range for a given load. Green indicates values within this range. Red indicates values outside this range. *Estimated.

| **Foot** | **Load** | | | |
|---|---|---|---|---|
| **Inversion** | **100 ± 1N** | **300 ± 1N** | **500 ± 1N** | |
| VF – Cat. 5 | -3.84 ± 0.07 | -7.47 ± 0.03 | -9.42 ± 0.02 | **Displacement [mm]** |
| VF – Cat. 8 | -3.60 ± 0.06 | -7.10 ± 0.03 | -8.92 ± 0.03 | |
| FI – Cat. 4 | -3.04 ± 0.07 | -7.10 ± 0.04 | -9.32 ± 0.04 | |
| FI – Cat. 8 | -3.06 ± 0.04 | -6.59 ± 0.03 | -8.87 ± 0.02 | |
| CSA – #3 – Stiff | -3.83 ± 0.07 | -7.91 ± 0.03 | -10.07 ± 0.02 | |
| CSA – #3– Compliant | -6.48 ± 0.07 | --- | --- | |
| CSA – #1 – Stiff | -3.53 ± 0.04 | -6.69 ± 0.02 | -8.48 ± 0.02 | |
| CSA – #1 – Compliant | -4.57±0.07 | -8.68 ± 0.05 | -10.82 ± 0.01 | |
| **Eversion** | | | | |
| VF – Cat. 5 | -3.43±0.08 | -7.25 ± 0.03 | -9.24 ± 0.05 | |
| VF – Cat. 8 | -3.16±0.06 | -6.66 ± 0.03 | -8.58 ± 0.03 | |
| FI – Cat. 4 | -4.77 ± 0.10 | -9.22 ± 0.10 | -12.55* | |
| FI – Cat. 8 | -2.76±0.04 | -6.87 ± 0.04 | -9.47 ± 0.03 | |
| CSA – #3 – Stiff | -3.49±0.06 | -7.13 ± 0.04 | -9.33 ± 0.02 | |
| CSA – #3 – Compliant | -4.27±0.12 | --- | --- | |
| CSA – #1 – Stiff | -3.02±0.06 | -6.42 ± 0.04 | -8.36 ± 0.02 | |
| CSA – #1 – Compliant | -3.27±0.08 | -7.25 ± 0.04 | -9.72 ± 0.03 | |

For the 500N loading condition, the majority of commercial devices fell within the stiffness range of the CSA. However, the eversion of the Freedom Innovations Sierra was more compliant. Under smaller loads, fewer devices fell within the range, an indication that the overall shape of the stiffness curve for some of the commercial devices was different than that of the CSA.

While the feet are symmetrical about the sagittal plane, there is a difference in stiffness for the same device in inversion and eversion. This is likely due to the interaction of the cosmesis with the foot based on whether the larger first phalange makes contact first, or the smaller fifth phalange.

### *Cart Position Control Characterization*

The motor proved to be insufficient for driving the cart up and down the CSA while loaded to 1000N in either inversion or eversion of 15 degrees. This was most likely due to the excessive deflection of the guide rods and ACME screw while loaded in such a manner. Even though the deflection is well within the elastic strain for the materials, any noticeable deflection greatly increases the friction of the system. Another possibility is that the brushless motor doesn't have enough starting torque, especially when compared to brushed motors with similar specifications though this difference is not as significant when Hall effect sensors are used by the motor controller.

For unloaded and vertically loaded conditions, data was collected successfully. The following is a sample plot of the data collected for the unloaded 12.7mm traverse. The vertical axis refers to the number of turns of the ACME rod. With a ¼-20 rod, 10 turns is equal to 12.7mm. In this example, the controller was programmed to start at the zero position – most compliant – move to ten turns down at full speed, move back to the 0.5 turn position at full speed, pause for one second and repeat the process indefinitely. Figure 17 shows the plot of the first four cycles.

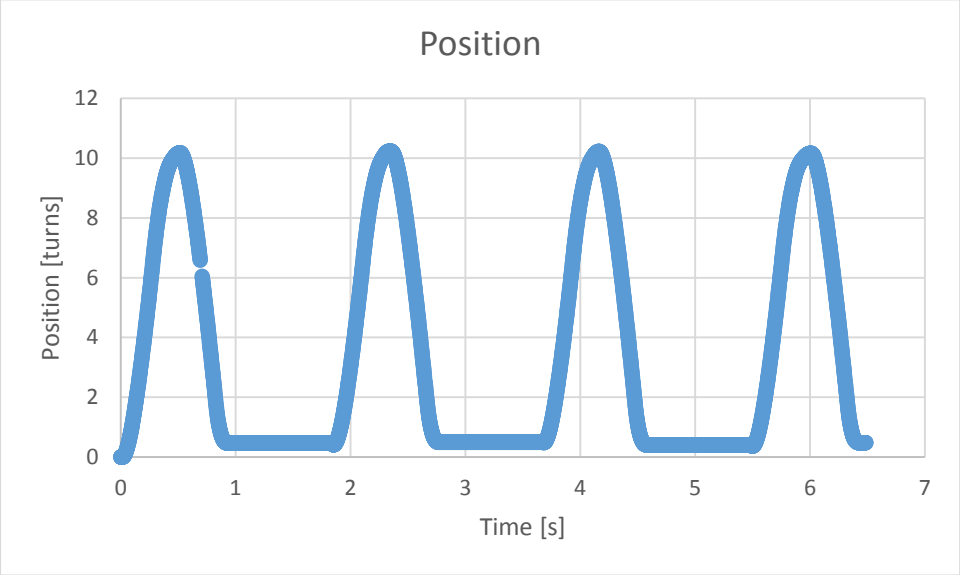


Figure 17: Position over time data for 10 turns, no load.

As can be seen in the figure, the total moving time for each cycle is less than one second. Table 7 shows total time per cycle.

Table 8: Turns and loading conditions testing motor speed.

| | **10 turns** | **30 turns** |
|---|---|---|
| **Unloaded** | 0.9 s | 1.9 s |
| **Vertically Loaded – 1000N** | 0.9 s | 2.0 s |

The change in stiffness can be compared to these turns. By curve fitting a polynomial to the data collected during the spring characterization, these turns can be equated to ankle stiffness values. Figure 18 shows the fourth order polynomial curve fitting based on the data from the CSA with the #1 spring set. The fourth order polynomial was chosen due to its close fit with the data, but is not a theoretically accurate description of the system since the spring stiffness would go to infinite as the effective length went to zero. However, for the purpose of understanding the stiffness qualities along the useable length of the cantilever beams, it is sufficient.

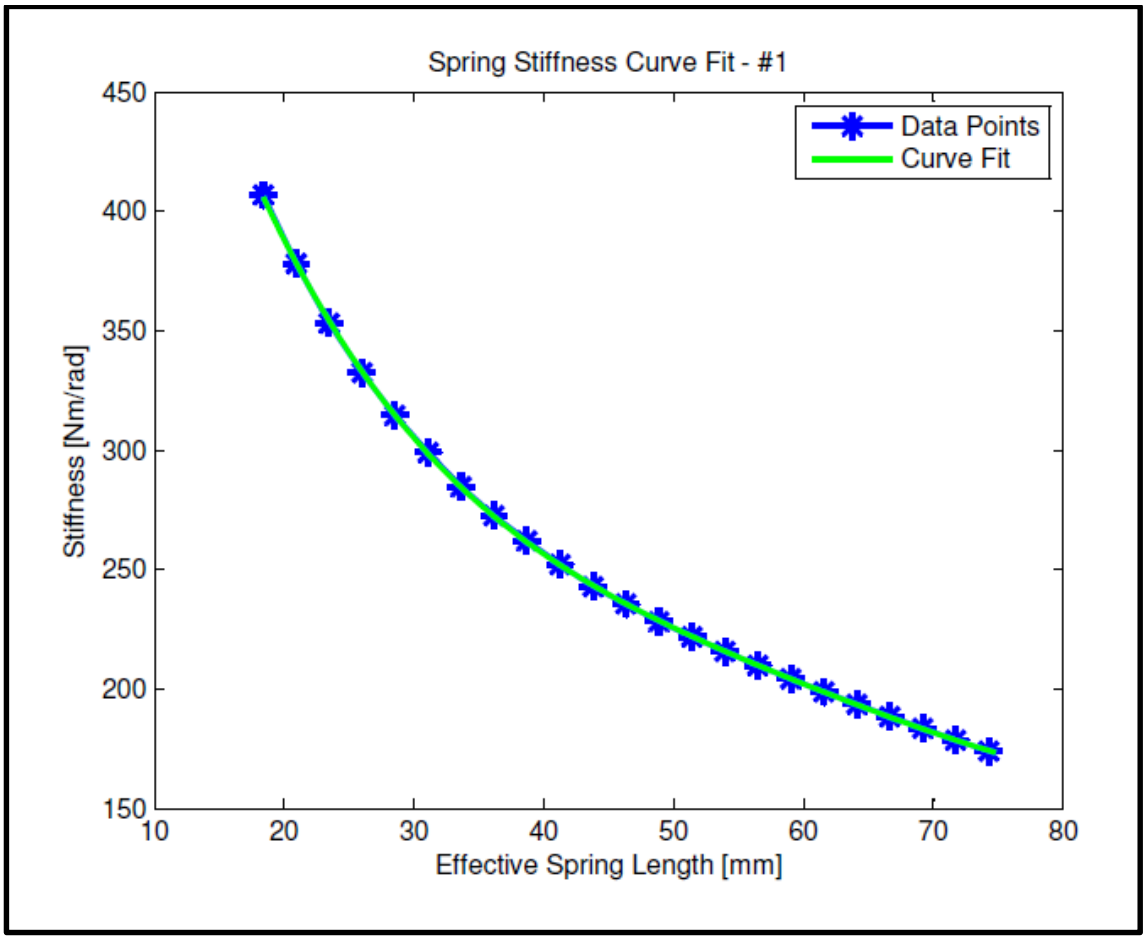


Figure 18: Polynomial curve fit to stiffness data points from the CSA #1.

The equation for this curve follows the form $k = Al^4 + Bl^3 + Cl^2 + Dl + E$ where $k$ is the stiffness measured in Nm/rad and $l$ is the effective length of the cantilever beam spring measured in mm.

Table 9: Stiffness curve fit coefficients for spring #1.

| Coefficient | Value |
|---|---|
| A | $2.578 * 10^{-5}$ |
| B | $-6.40 * 10^{-3}$ |
| C | $0.6045$ |
| D | $-28.079$ |
| E | $754.808$ |

This means that a change in ten turns at different points along the spring causes different changes in stiffness. For example, ten turns from the most compliant to stiffer results in a change of approximately 28 Nm/rad. Ten turns from more compliant to the stiffest value result in a change of 118 Nm/rad. When the turns over time plot of figure 17 is changed to represent the potential changes in stiffness, the plots appear as seen in figure 19. For ten turns, the maximum change is 39%. For thirty turns, the maximum change is from 212 Nm/rad to 437 Nm/rad or a change of 106%. For half of a one second gait cycle, the CSA with the #1 spring set can change angular stiffness by approximately 118Nm/rad.

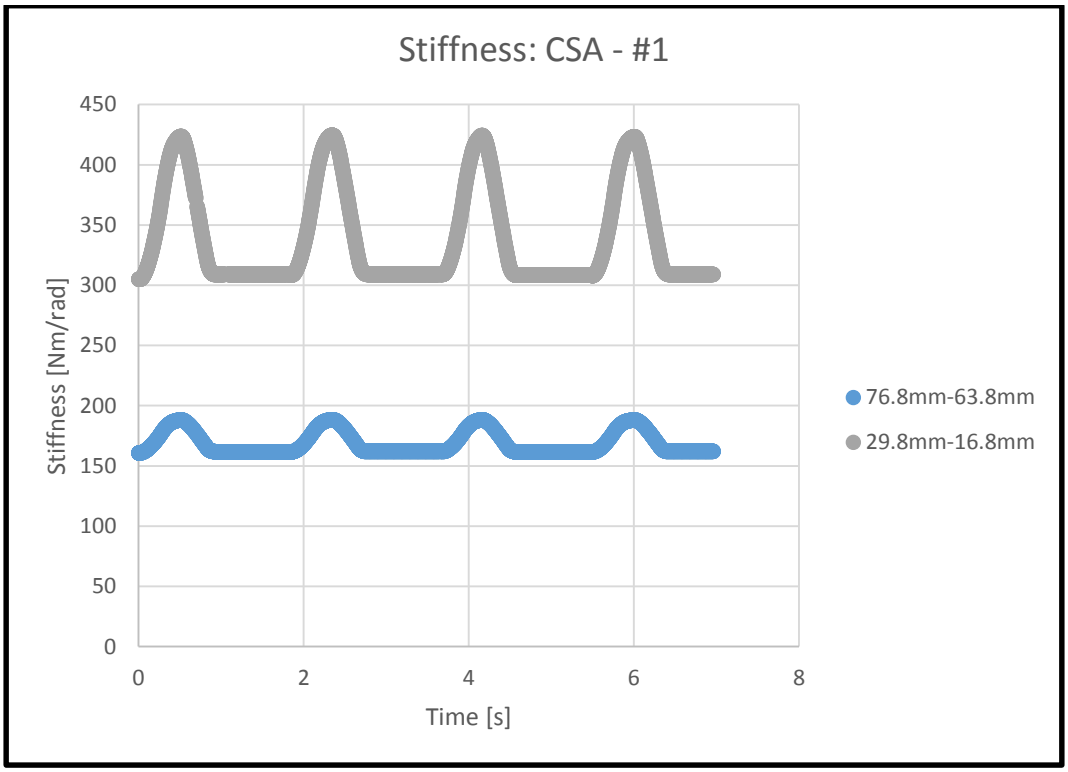


Figure 19: Change in stiffness over time for the 10 turn motor test.

## 3.2 Human Subject Testing

### *Standing Balance Test*

The data collected during the standing balance test was the position of the COP on the force plate over time. The data was truncated to the middle 40 seconds of the 60 second data collection to eliminate starting and ending artifacts in the data. Figure 20 shows a sample plot of the COP path, centered about the mean

position. The red '+' symbols indicate the standard deviation in the x and the y directions and the letters represent anterior, posterior, right and left directions of the test subject.

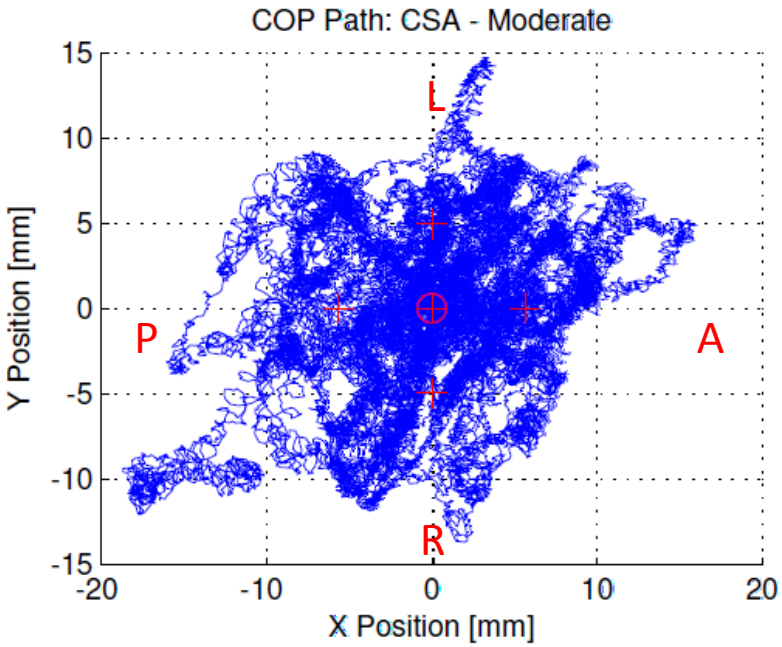


Figure 20: Tracking x-y coordinates of the CoP for the CSA at moderate stiffness. (L)eft; (A)nterior; (R)ight; (P)osterior

When two of these plots are compared, one can see a difference between the COP paths. In figure 21, there is a noticeable difference between the COP path of the rigid pylon ankle with the Össur Vari-Flex LP category 9 foot and the COP for the prescribed Össur Vari-Flex category foot.

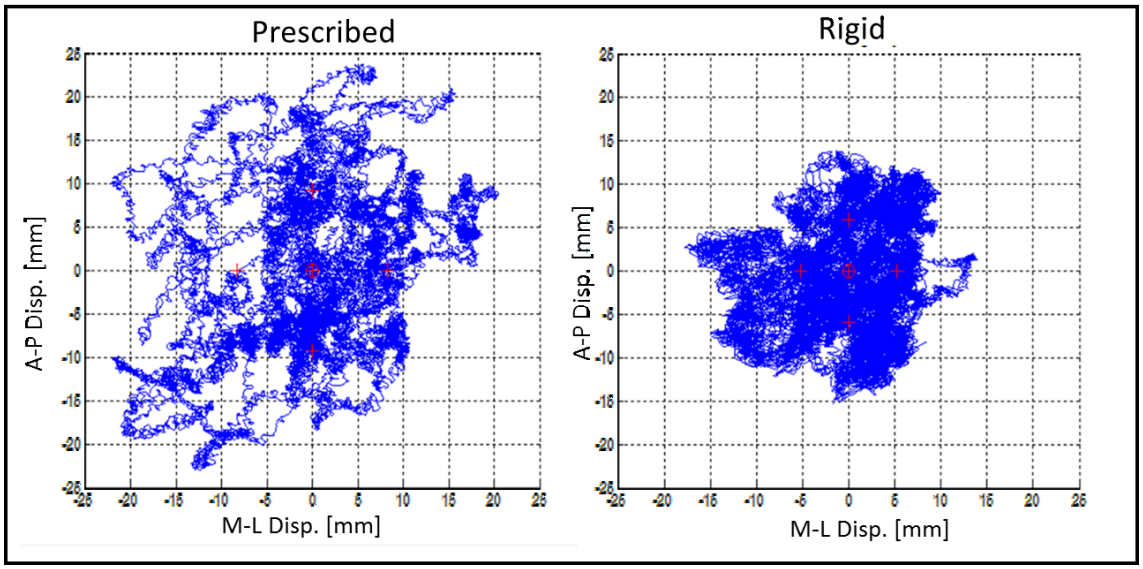


Figure 21: COP path comparison between the most variable (Prescribed) and the least variable (Rigid).

The displacement can then be separated into medial/lateral (ML) displacement and anterior-posterior (AP) displacement. For both of these, the prescribed device showed the greatest range of displacement. Also, as the stiffness of the CSA increased, the ML displacement decreased. This can be seen in figures 22 and 23.

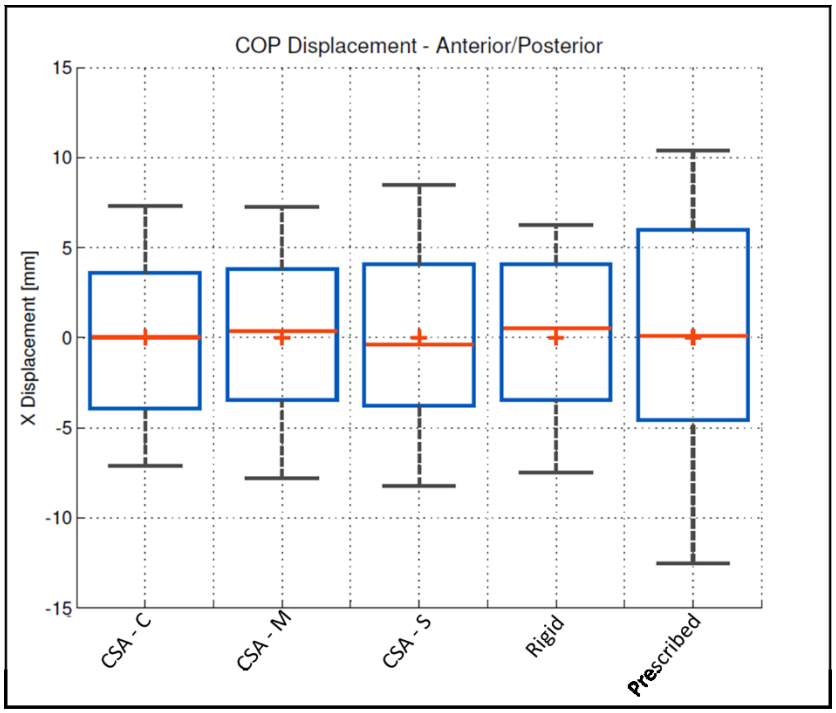


Figure 22: COP anterior and posterior displacement. The red cross indicates the median, the read line the mean, the blue box the 25%-75% data range and the whiskers 5-25% and 75-95% data ranges

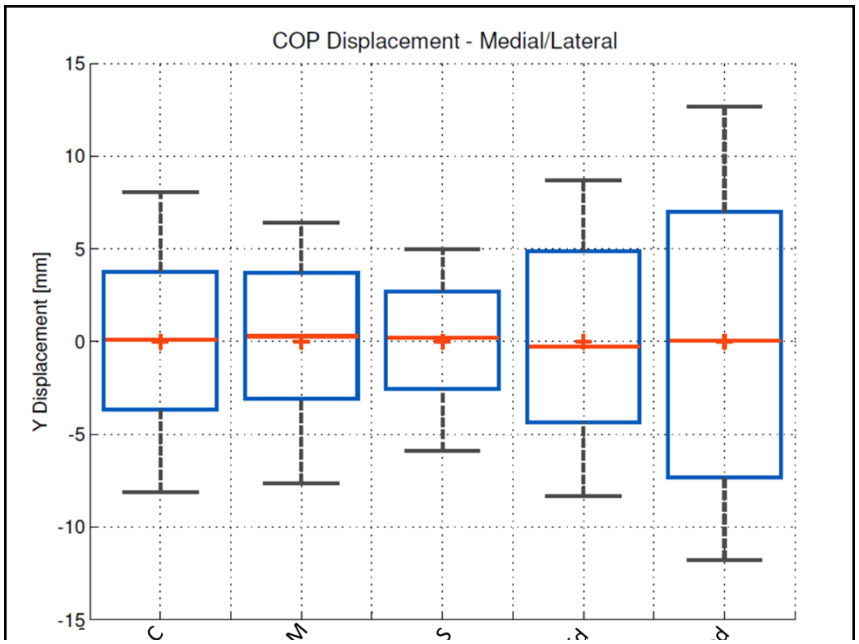


Figure 23: COP medial and lateral displacement. There is a noted decrease from the most compliant to the stiffest CSA settings.

Another metric for evaluating the COP was the velocity. The velocity of the rigid pylon was much greater than any of the other foot and ankle combinations, but there was no noticeable difference between the different CSA stiffness values as is shown in figure 24. These results are quantified in table 10.

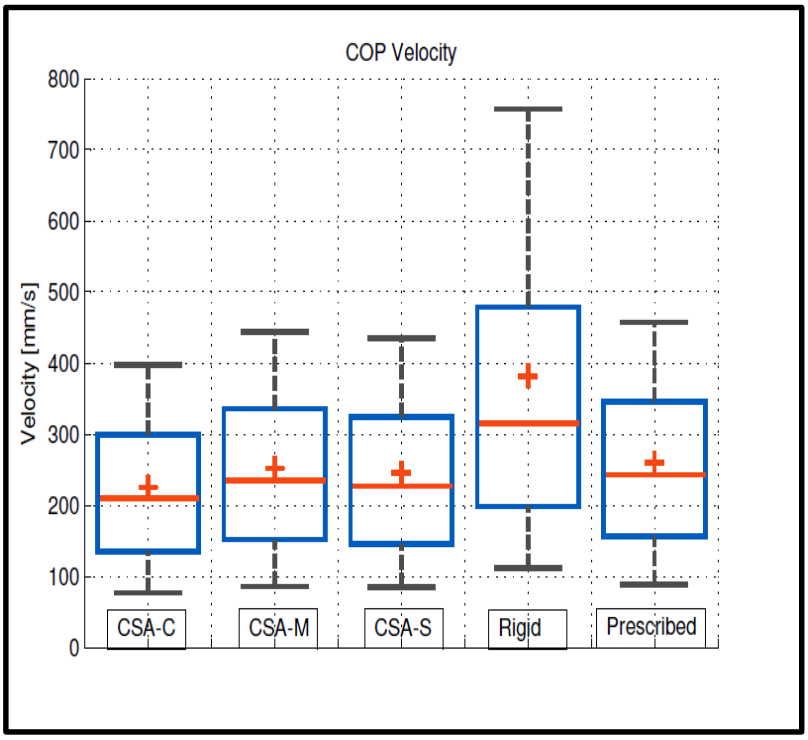


Figure 24: Velocity of COP showing that the rigid pylon had a much greater velocity than the other any of the others.

Table 10: CoP standard deviation and average velocity.

| | **Position Standard Deviation [mm]** | | **Average Velocity [mm/s]** | |
|---|---|---|---|---|
| **Ankle** | Sagittal | Coronal | Sagittal | Coronal |
| CSA-Compliant | 5.5 | 5.9 | 261.3 | 286.2 |
| CSA-Moderate | 5.6 | 4.9 | 239.2 | 279.2 |
| CSA-Stiff | 6.3 | 4.2 | 271.7 | 289.8 |
| Rigid Pylon | 5.2 | 6.0 | 263.7 | 284.4 |
| Prescribed | 8.3 | 9.3 | 236.1 | 292.6 |

The rigid pylon with the category 9 foot tended to have short fast motions that were generally centered. The prescribed foot tended to have wide slow motions. The CSA tended to have small slow motions. The three different stiffness values of the CSA showed little difference in these characteristics, though there was a noted decrease in coronal plane sway from the most compliant to the stiffest setting.

*Walking on Uneven Terrain*

Three main metrics were used to evaluate how the CSA affected gait on uneven surfaces. The first was the angle of the ankle during the foot placement. The second was the moment about the ankle. The third was the relative stiffness of the ankle throughout the gait cycle.

The only obvious effect seen in the graphs is the change in ankle angle in the coronal plane. The coronal ankle moment has no readily observable differences between the three conditions, though there does seem to be some peak for the stiffest position at heel strike and toe-off. Unfortunately this does not support the hypothesis that making an ankle conform to an inverted or everted plane more would make a difference to the moment at the ankle. Since the ankle is bending more, this changes moment arms in the system and must somehow change how the device is interacting with either the ground, the individual or both.

The stiffness evaluated from the data shows that the actual stiffness values in the coronal plane through the gait cycle follow a very non-linear path, but do change generally for different settings on the CSA as a result of the ankle angles being different between the three cases.

Figures 25, 26 and 27 show these metrics for the stance portion of the gait cycle. Each line indicates one trial.

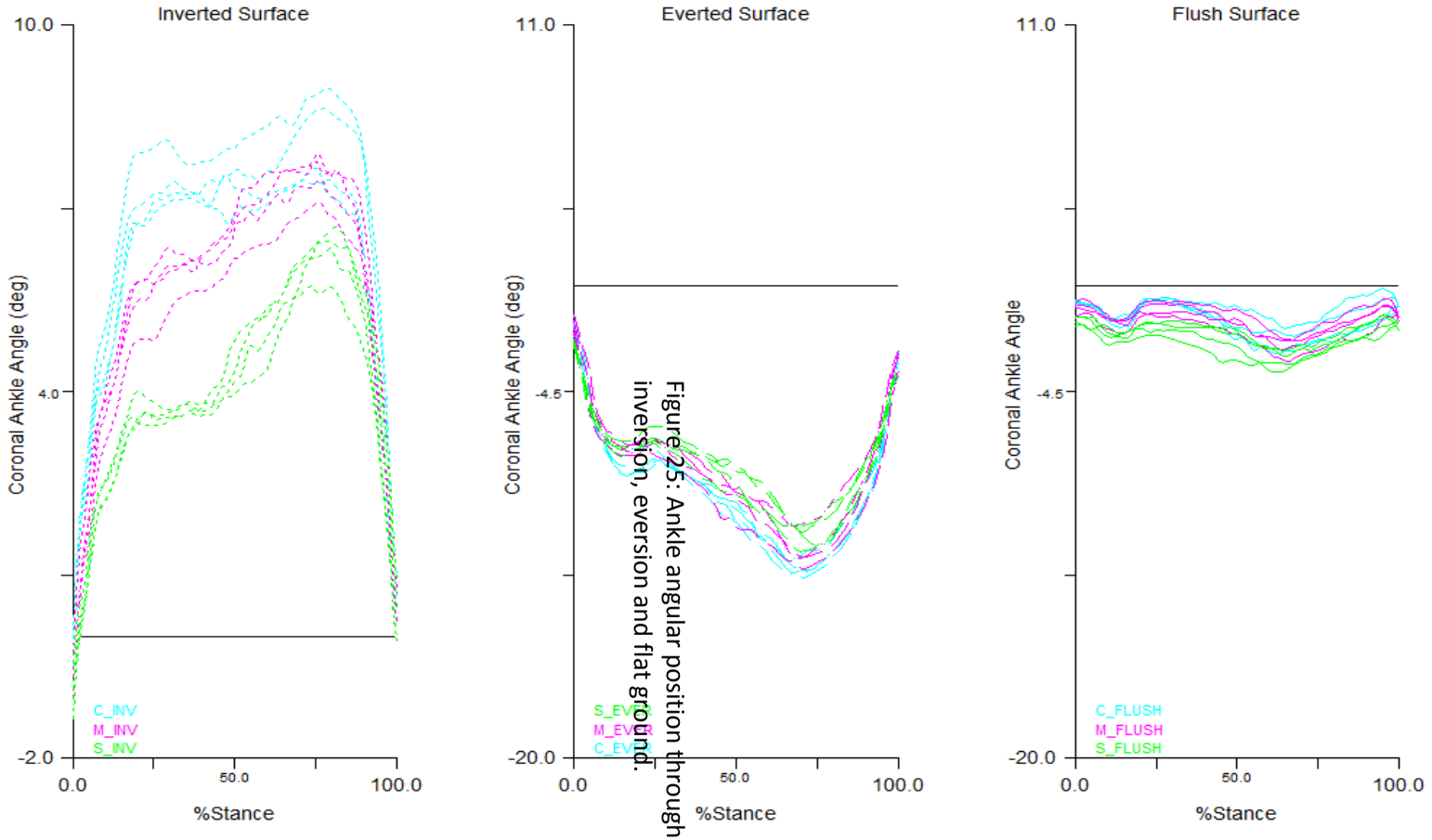


Figure 25: Ankle angular position through the stance phase of the gait cy
inversion, eversion and flat ground.

## Coronal Ankle Moments - CSA only

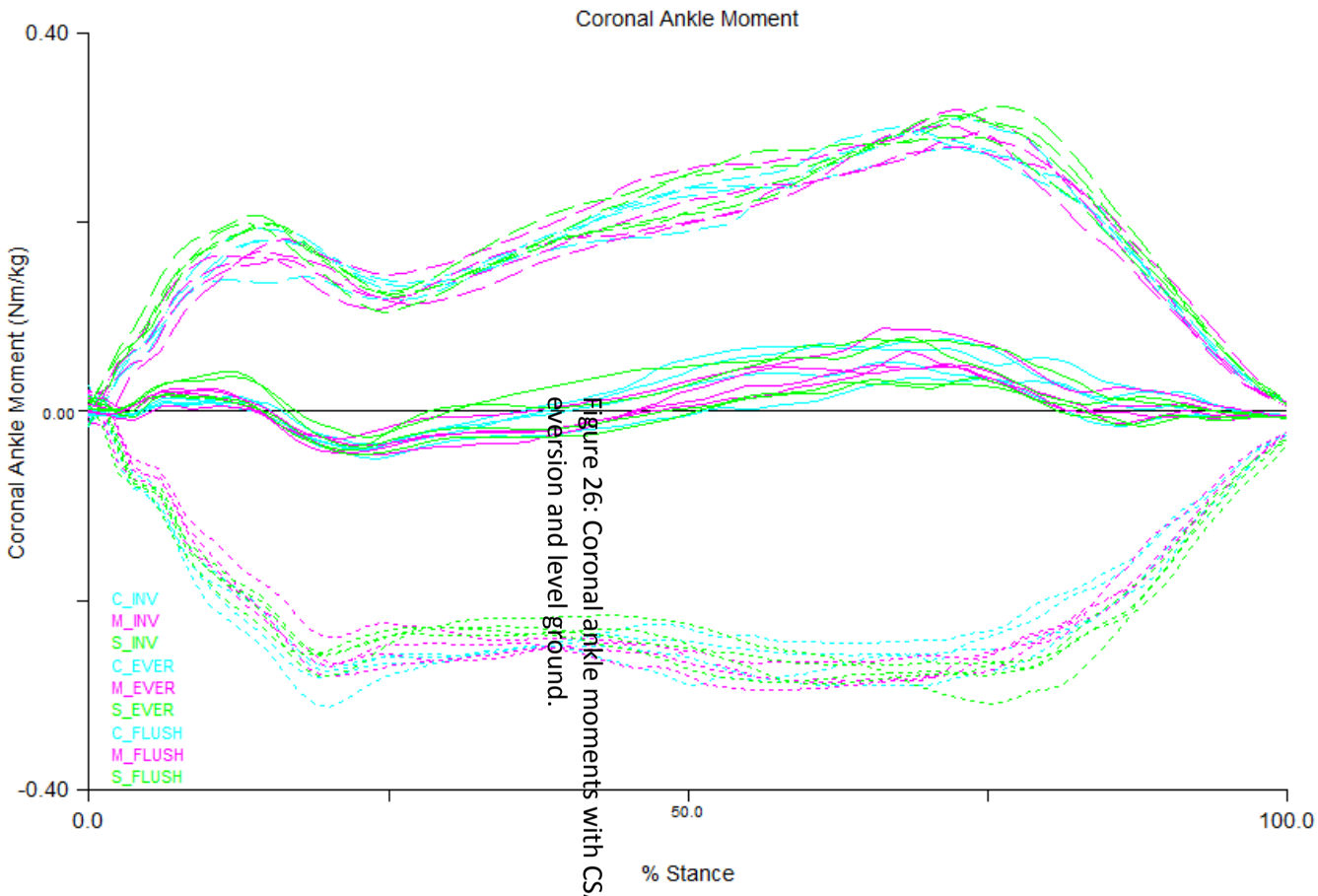


Figure 26: Coronal ankle moments with CSA at three different stiffn
eversion and level ground.

## Coronal Plane Stiffness

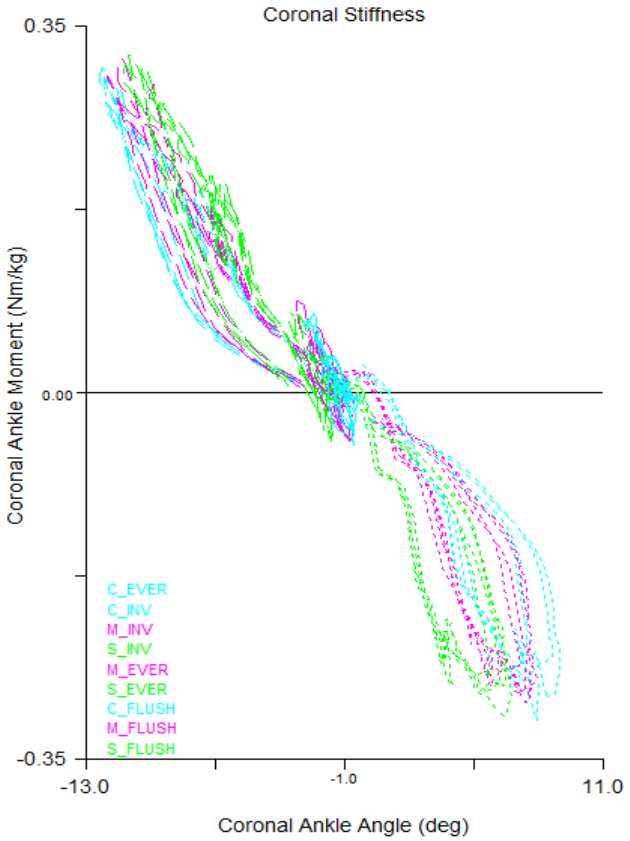


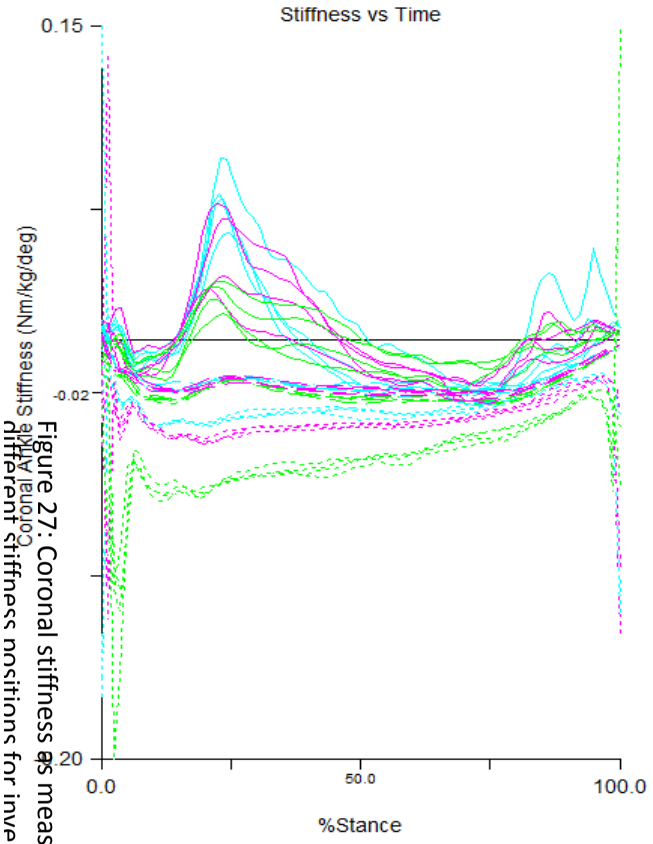


Figure 27: Coronal stiffness as measured about the ankle joint for the different stiffness positions for inversion, eversion and level ground

# 4 Discussion

The basic concept of a controlled stiffness inverting and everting prosthetic ankle has been proven. The device allows for a wide range of stiffness values. A moderate stiffness spring set has a range of stiffness equivalent to a wide variety of commercial device stiffness categories. The device has also proven that it is structurally sufficient for walking on level terrain and uneven terrain. The drive mechanism for changing the stiffness is sufficient for changing the stiffness quickly over a wide range when the ankle is loaded vertically, but not when it has a full bodyweight moment applied due to inversion or eversion. The device currently has no input, but has the capability for implementing control loops based on loading and gait position analysis.

Bench testing has shown physical characterization of the device, but further testing is needed to determine how the device can best improve amputees' ability to traverse uneven terrain. The motor control tests require improvements to work while fully loaded, but the rate of stiffness change is already significant with up to 39% increase in stiffness in less than 0.5 seconds.

Initial results from the sway test show interesting characteristics indicating that there may be an optimal stiffness for minimizing sway while standing – rigid pylons with stiff feet create high velocity motions and more compliant feet create large motions. The numerical results can be compared to previous studies under similar conditions. One such study reported similar excursion in the medial-lateral and anterior-posterior. In this study, the greatest range was with the prescribed device – 47.5mm AP, 43mm ML. The smallest range was with the rigid pylon and category 9 foot – 29.5mm AP, 30mm ML. This is compared to similar conditions resulting in 35.7mm AP and 28.6mm ML from a 24 subject study [24].

The results of the dynamic walking over the inverted and everted force plate show that changing the stiffness of the CSA effectively changes the ankle angle. Based on this change in angle, one might expect a measurable change in the moment about the ankle, however, no difference was readily observable. This may be a result of moments being transferred to the deformation of the liner and soft tissues of the residual limb, or somehow compensated by non-linear material characteristics in the shoe and cosmesis that would be compressed in different manners with different applied loads.

# 5 Future Work

Further improvements can be made to the device. To begin with, it is important that the device be able to change stiffness characteristics while the limb is loaded on an inverting or everting slope. Currently, the device cannot do this. Excessive deflection of the guide rods seems to be a primary cause, so retrofitting the ankle with a more rigid roller guide system may help to alleviate this issue. Another option is using a motor with more starting torque as long as the speed requirements are still fulfilled.

To begin changing the stiffness characteristics throughout the gait cycle, one must know where in the cycle the user is at any given time. This can be done with a simple gait characteristic detection system using gyroscopes and accelerometers as explained in Appendix B. Another means of controlling the system is reacting to input moments. These could be detected by in-line force sensors that would be able to determine the applied force and moments, or by measuring the angular displacement in relation to the known stiffness of the spring. A potentiometer is already included in the current control system, although this was not implemented during the human subject testing. For better precision with small angles, another device would be a magnetic angular position sensor such as those commonly found in the automotive industry.

Another area of interest would be using springs with varying cross-sections along their length. For example, a spring that tapers would have a broader range of stiffness over the same change in length than the straight springs that were used. If the ideal stiffness profile were identified, this could be simulated through the change in geometry of the springs. More significant stiffness changes over a shorter change in length may require high precision location, but added benefits would include possibly making the device shorter and more light weight. This would make the device potentially more practical for a wider variety of subjects.

Beyond mechanical improvements, a few other aspects should be investigated to realize the potential of the CSA as a research instrument. The first is to thoroughly investigate what amputees want and need for stability on uneven terrain. This may best be accomplished by using the Zero Moment Point as a measurable metric as well as determining the moments applied to the residual limb. One hypothesis is that the foot should conform to the terrain such that the path of the ZMP relative to the center of gravity follows the same trajectory as walking on level ground which would improve amputee confidence [22, 23]. Another

hypothesis is that with the foot conforming to uneven terrain, the applied moment on the residual limb will be less than what would occur with a more rigid system and thus would decrease fatigue.

# Appendix A – Device Design

The description of this device is broken down into three areas, the mechanics, the electronics and the control. For each section, the relevant functional pieces are identified and a brief description is given as to their purpose. At the end of each section is a brief description of improvements that could be made. At the end of the device description is a listing of other possible designs that were considered with pros and cons listed as well as the ultimate reasoning behind the final design selection.

## Mechanical Design

The upper shank of the Controlled Stiffness Ankle (CSA) rotates about a pin joint connecting it to the foot. Two cantilever beam springs hold the shank in an upright position until deflected by moments applied to the foot or shank about the pivot point. The point at which the load is applied to the spring is adjusted using a moving cart. All parts, unless otherwise noted, are machined from 7075 aluminum for its strength and low weight characteristics. Note: most dimensions are made to even fractions of inches.

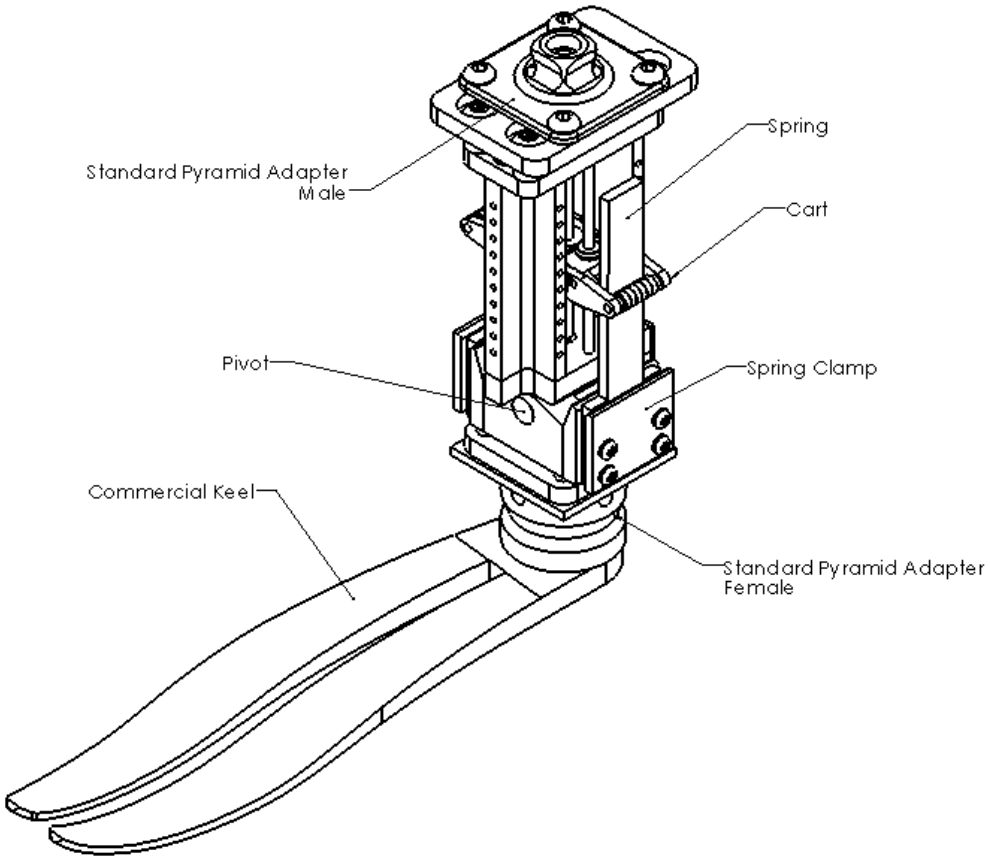


Figure 28: CSA drawing

The standard pyramid adapter has a standard four bolt hole pattern threaded for M6x1 screws spaced 36mm center to center on an edge. Adapters tend to use flat head socket screws rather than the button head socket screws shown in the diagram.

A close-up of the drive mechanism is shown below in figure 25 with the top adapter and adapter plate removed. The adapter plate is offset above the gears with stainless steel spacers.

Transmission Gears:

SDP-SI # S1063Z-064S080 – Pitch: 64, Teeth: 80, Material: 303 SS, Pressure Angle: 20°

Motor:

Maxon Motors #400160 – 30W brushless

Motor Gearhead:

Maxon Motors #110321 – 4.4:1

Maxon #138335 – 19:1

The transmission gears are attached to their respective shafts with setscrews on flats. The motor is attached to the main shank with a metal strap, clamping the motor to a bumper. The motor bumper serves three purposes. It allows for positioning of the motor shaft in precisely as needed for the gear size. It also reduces the vibrations from the motor to the shank. Lastly, it can act as a clutch allowing the motor to slip if overwhelming torques are applied to the system. While this does not occur under ordinary operating circumstances, preventing damage to the motor, gears or clamps is important.

Also shown in this figure is one of the uprights. These are the main frame of the shank, transferring loads from the top adapters to the base plate. The uprights have a number of #2-56 threaded holes to accommodate future sensor expansion, battery attachment, micro-controller attachment and other devices that may later be used to expand the capacity of the device.

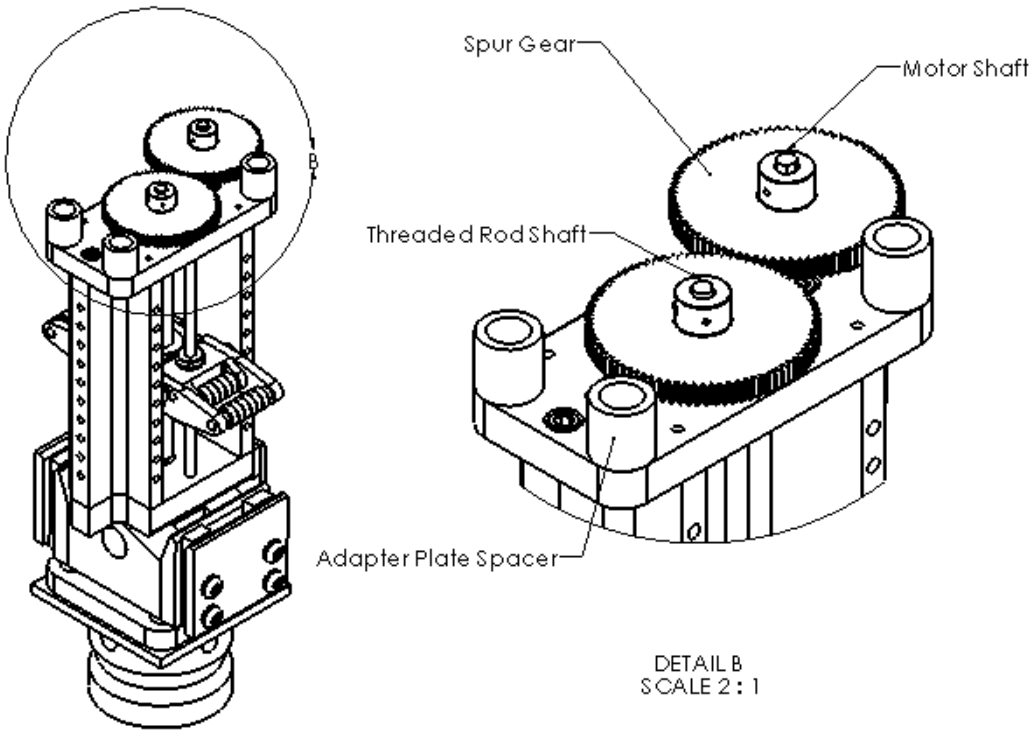


Figure 29: Drive mechanism for ACME rod.

Spur gears were chosen over a belt or chain drive system due to their small profile and a wide variety of sizes were readily available. Also, the consistency of positioning with spur gears does not have to worry about stretching as in belts or chains.

The drive mechanism turns a ¼-20 ACME screw. A high precision ACME screw was chosen for its availability, lower friction and tight tolerances. The size was chosen to minimize size since the driving forces of the screw would not be extreme. The pitch was chosen to prevent back-driving as determined by the

coefficient of friction between the stainless steel rod and the brass nut. Ball-screws were not selected because they are easily back-drivable. The ACME rod is held in position by two rotary ball bearings, one at either end.

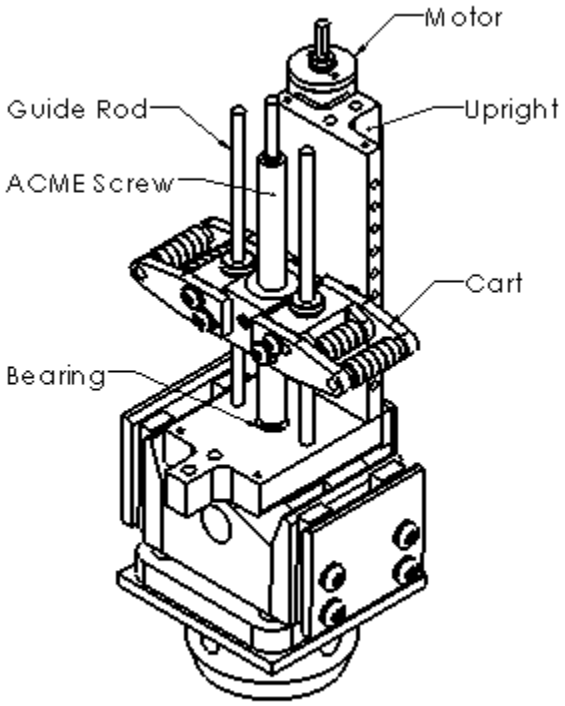


Figure 30: Cart positioning system

The ACME nut is fixed in the cart with a hard stop in the direction of the greatest force (on the bottom) and two set screws to keep it from rotating or sliding up in the housing. The cart also has two linear bearings that slide up and down the guide rods of the shank. These linear bearings are also held in place with set screws. The two guide rods prevent the cart from rotating and thus limit the cart to a linear motion up and down when the threaded rod is turned. The guide rods also transfer the applied moments of the shank to the cart which in turn applies them to the springs.

The other features of the cart are the bearings that ride on either side of each spring set. These bearings allow the cart to slide up and down the springs even when radial forces are applied to them such as when

the spring is under loading. The outer set of bearings is adjustable to accommodate different spring thickness. The outer bearings are held in place by arms that are clamped to the main cart body by two screws each. Because of the considerable forces applied to the arms via the bearings, the simple clamping forces of the screws would not be sufficient to hold them in place. Therefore, the faces between the cart body and the arms are knurled with a linear pattern so as to greatly increase the friction of the interface. This knurling limits the arms to discrete positions, but due to the close spacing of the knurling, this did not prove to be a limitation with the spring sets tested.

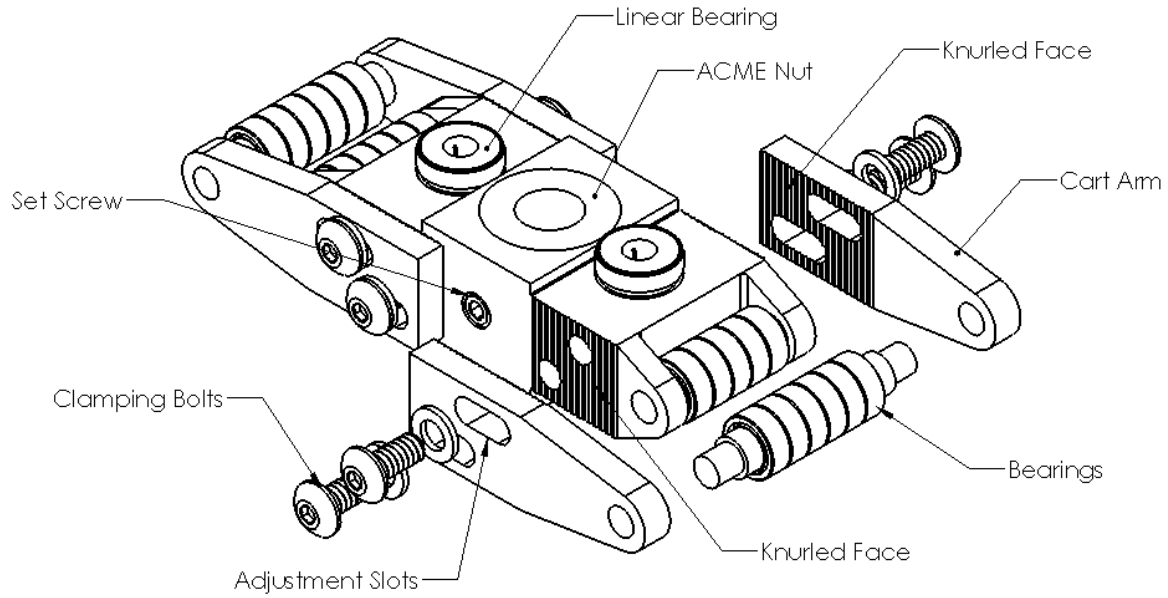


Figure 31: Cart features

The lower end of the threaded rod and the guide rods sit in the base block. This base block also supports the uprights. On the bottom flange of the base block is the hole for the pivot. Originally, this had a needle bearing that was later replaced with a lubricated bronze bushing to eliminate the angular displacement of the pivot axis due to the slop in the bearing.

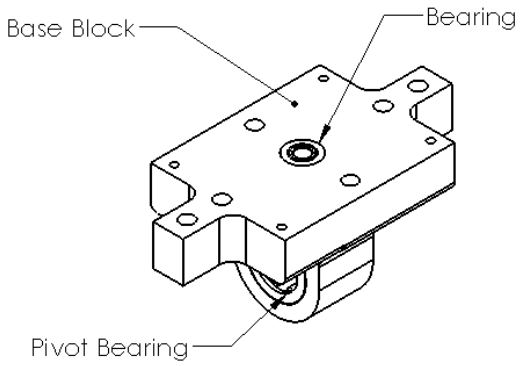


Figure 32: Base block features

The foot of the device consists of the foot block and the spring clamps. The foot block contains the pivot which is held in place with a press fit. The pivot is made of precision ground, hardened stainless steel. Both the clamp face and the clamp back are attached to the foot block with screws. Both have a rounded top edge where they make contact with the deflecting beam to prevent sharp edges breaking the carbon fiber laminate. Between the clamp face and the clamp back is the spacer, made from the same material as the spring. Because the spacers and the spring are the same thickness, a small shim (0.003-0.012”) is placed on the spring face to create more of a clamping force when the screws are tightened.

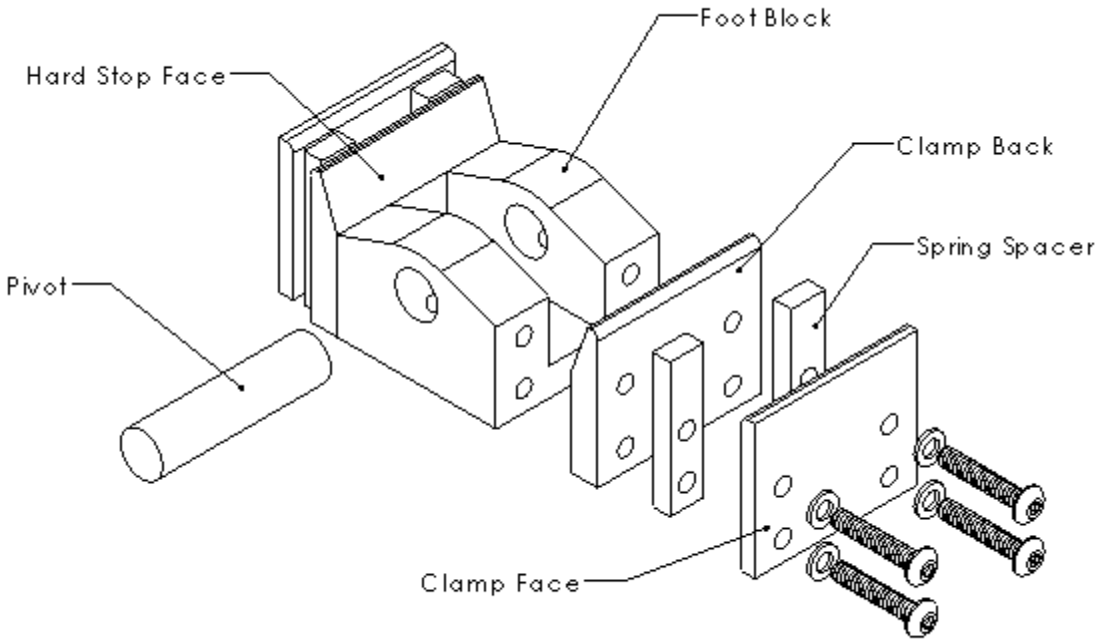


Figure 33: Detail of foot block and spring clamps

The cantilever beam springs of the device are made from carbon fiber laminate (8194K12, McMaster-Carr, Los Angeles, CA) of varying thickness cut to 16.5x105mm.

# Bibliography


[1] T. R. Dillingham, L. E. Pezzin, E. J. MacKenzie, A. R. Burgess, “Use and satisfaction with prosthetic devices among persons with trauma-related amputations: a long-term outcome study.” *American Journal of Physical Medicine and Rehabilitation,* vol. 80, no. 8, pp. 563-571, Aug. 2001.

[2] M. W. Legro, G. Reiber, “Issues of importance reported by persons with lower limb amputations and prostheses.” *Journal of Rehabilitation Research and Development,* vol. 36, no. 3, pp155, Jul. 1999.

[3] W. C. Miller, A. B. Deathe, M. Speechley, J. Koval, “The influence of falling, fear of falling, and balance confidence on prosthetic mobility and social activity among individuals with a lower extremity amputation.” *Physical Medicine and Rehabilitation,* vol. 82, no. 9, pp. 1238-1244, Sep. 2001.

[4] C. J. C. Lamoth, E. Ainsworth, W. Polomski, H. Houdijk, “Variability and stability analysis of walking of transfemoral amputees.” *Medical Engineering and Physics*, vol. 32, no. 9, pp.1009-1014, Nov. 2010.

[5] S. Siegler, J. Chen, C.D. Schneck, “The three-dimensional kinematics and flexibility characteristics of the human ankle and subtalar joints – Part I: Kinematics.” *Journal of Biomechanical Engineering*, vol. 110, no. 4, pp 364-373, Nov. 1988.

[6] R. Kakkar, M.S. Siddique, “Stresses in the ankle joint and total ankle replacement design.” *Foot and Ankle Surgery,* vol. 17, no 2, Jun. 2011.

[7] K. Shamaei, G.S. Sawicki, A.M. Dollar, “Estimation of Quasi-Stiffness and Propulsive Work of the Human Ankle in the Stance Phase of Walking.” *PLoS One,* vol. 8, num. 3, Mar. 2013.

[8] T. Kobayashi, A.K.L Leung, S.W. Hutchins, “Design of a manual device to measure ankle joint stiffness and range of motion.” *Prosthetics and Orthotics International,* vol. 35, no. 4, pp 478-481, Dec. 2011.

[9] L. Charalambous, G. Irwin, I. Bezodis, D. Kerwin, “Lower limb joint kinetics and ankle joint stiffness in the sprint start push-off.” *Journal of Sports Science*

[10] S. M. Zinder, K. P. Granata, D. A. Padua, B. M. Gansneder, “Validity and reliability of a new in vivo ankle stiffness measurement device.” *Journal of Biomechanics.* Vol. 40, no. 2, pp. 463-467, 2007.

[11] H. Lee, P. Ho, M. A. Rastgaar, H. I. Krebs, N. Hogan, “Multivariable static ankle mechanical impedance with relaxed muscles.” *Journal of Biomechanics.* Vol. 44, no. 10, pp 1901-1908, July, 2011.

[12] K. Tao, D. Wang, C. Wang, X. Wang, A. Liu, C.J. Nester, “An in vivo experimental validation of a computational model of human foot.” *Journal of Bionic Engineering*, vol. 6, no. 5, pp. 387-397.

[13] D.L.A. Camacho, W.R. Ledoux, E.S. Rohr, B.J. Sangeorzan, R.P. Ching, “A three-dimensional, anatomically detailed foot model: A foundation for a finite element simulation and means of quantifying foot-bone position.” *Journal of Rehabilitation Research and Development,* vol. 39, pp. 401-410, 2002.

[14] “AOPA Prosthetic Foot Project Report” *American Orthotic and Prosthetic Association*, Sept. 2010.

[15] A. Banerjee, B. Bhattacharya, A.K. Mallik, “Large deflection of cantilever beams with geometric non-linearity: Analytical and numerical approaches.” *International Journal of Non-Linear Mechanics*. Vol. 43, no. 5, pp. 366-376, June 2008.

[16] J.A. Raymakers, M.M. Samson, H.J.J. Verhaar, “The assessment of body sway and the choice of the stability parameter(s).” *Gait and Posture*, vol. 21, no. 1, Jan. 2005.

[17] D. Rusaw, K. Hagberg, L. Nolan, N. Ramstrand, “Can vibratory feedback be used to improve postural stability in persons with transtibial limb loss?” *Journal of Rehabilitation Research and Development*, vol. 49, no. 8, pp. 1239-1254, 2012.

[18] S. Uimonen, K. Laikatari, M. Sorri, R. Bloigu, A. Palva, “Effect of positioning of the feet in posturography.” *Journal of Vestibular Research*, vol. 2, pp. 349-356, 1992.

[19] S. Wolf, J. Simon, et al. “Foot motion in children shoes: a comparison of barefoot walking with shod walking in conventional and flexible shoes.” *Gait Posture*, vol. 27, no. 1, pp. 51-59, 2008.

[20] W.T. Dempster. “Space requirements for the seated operator.” *Wright Patterson Air Force Base* Ohio, WADC-TR-55-159, 1955.

[21] D.A. Winter, “The biomechanics and motor control of human gait: normal, elderly and pathological.” *University of Waterloo Press*, 1991.

[22] W. Suleiman, F. Kanehiro, K. Miura, E. Yoshida, “Enhancing zero moment point-based control model: system identification approach.” *Advanced Robotics*, vol. 25, no. 3, pp. 427-446, 2011.

[23] C.L. Shih, W.Y. Lee, C.P. Wu, “Planning and control of stable walking for a 3D bipedal robot.” *International Journal of Advanced Robotic Systems*. Vol. 9, no. 47, 2012.

[24] D. Rusaw, K. Hagberg, L. Nolan, N. Ramstrand, “Can vibratory feedback be used to improve postural stability in persons with transtibial limb loss?” *Journal of Rehabilitation Research and Development*, vol. 49, no. 8, pp. 1239-1254, 2012.